Multistep Sequential Mechanism of *Escherichia coli* Helicase PriA Protein−ssDNA Interactions. Kinetics and Energetics of the Active ssDNA-Searching Site of the Enzyme†

Roberto Galletto, Maria J. Jezewska, and Wlodzimierz Bujalowski*

Department of Human Biological Chemistry and Genetics, Department of Obstetrics and Gynecology, the Sealy Center for Structural Biology, Sealy Center for Cancer Cell Biology, The University of Texas Medical Branch at Galveston, 301 University Boulevard, Galveston, Texas 77555-1053

Received March 31, 2004; Revised Manuscript Received June 4, 2004

ABSTRACT: Kinetics of the *Escherichia coli* PriA helicase interactions with the ssDNA has been studied, using the fluorescence stopped-flow technique. Experiments have been performed with a series of fluorescent etheno derivatives of ssDNA adenosine oligomers, differing in the number of nucleotide residues. The PriA helicase binds the ssDNA in the sequential process defined by

$$\text{PriA} + \text{ssDNA} \underset{k_{-1}}{\overset{k_1}{\rightleftarrows}} (\text{P})_1 \underset{k_{-2}}{\overset{k_2}{\rightleftarrows}} (\text{P})_2 \underset{k_{-3}}{\overset{k_3}{\rightleftarrows}} (\text{P})_3$$

In the first step, the enzyme associates fast with the ssDNA without inducing conformational changes in the DNA. The dependence of the partial equilibrium constant, characterizing the first step, upon the length of the ssDNA strictly reflects the statistical relationship between the size of the DNA-binding site and the number of potential binding sites on the ssDNA. Only the DNA-binding site that encompasses 6.3 ± 1 residues is directly involved in interactions. The site is located on a structural domain allowing the enzyme to efficiently search and recognize small patches of the ssDNA. Intramolecular steps are independent of the ssDNA length and accompanied by changes in the DNA structure. Salt and glycerol effects on the studied kinetics indicate a very different nature of the intermediates. While the bimolecular step is characterized by net ion release and water uptake, net ion uptake and water release accompany intramolecular transitions. Specific ion binding stabilizes the helicase−ssDNA complex in $(P)_2$ and $(P)_3$ intermediates. However, magnesium and AMP−PNP do not affect the mechanism of enzyme−ssDNA interactions. The sequential character of the mechanism indicates that the enzyme does not exist in a preequilibrium conformational transition *prior* to the DNA binding.

The PriA helicase is a DNA replication enzyme in *Escherichia coli* that plays a fundamental role in the ordered assembly of the primosome, a multiple-protein−DNA complex formed in the process of priming a DNA strand (*1*−*3*). The primosome can translocate along the DNA while synthesizing short oligoribonucleotide primers, used to initiate synthesis of the complementary strand (*1*−*3*). Both PriA and DnaB helicase activities are involved in the primosome functioning. Originally, the PriA helicase was discovered as an essential factor during the synthesis of the complementary DNA strand of phage ΦX174 DNA (*4*, *5*). Recent data indicate that the enzyme is involved not only in DNA replication but also in recombination and repair processes in the *E. coli* cell (*2*, *6*−*16*). The gene encoding the PriA protein has been cloned and sequenced, and that of the encoded protein has been determined (*13*, *14*).

In vivo functions of the PriA helicase are related to the ability of the enzyme to interact with both single-stranded (ss) and double-stranded DNAs (dsDNAs). In these capacities, the enzyme is involved in interactions with specific DNA fragments, the primosome assembly site (PAS) and stalled replication forks (*3*, *7*−*10*, *15*−*18*). Equilibrium thermodynamic studies showed that the PriA helicase binds the ssDNA as a monomer, independent of the type of the nucleic acid base, type of salt, and salt concentrations, as well as the presence of nucleotide cofactors (*19*, *20*). Moreover, the affinity of the PriA monomer for the ssDNA is unaffected by the presence of nucleotide cofactors. Analyses of the helicase interactions with different ssDNA oligomers, over a large range of nucleic acid concentrations, indicate that the enzyme has a single ssDNA-binding site. The total site-size of the PriA−ssDNA complex, i.e., the maximum number of nucleotide residues occluded by the enzyme in the complex with the ssDNA, is $n_t = 20 \pm 3$ residues per protein monomer (*19*, *20*). However, the determined maximum number of nucleotides directly engaged in interactions with the ssDNA-binding site of the helicase is only $n = 8 \pm 1$, i.e., it is much smaller than the total site-size of the complex. Analysis of stoichiometries

† This work was supported by NIH Grant GM-46679 (to W.B.). R.G. was partially supported by J. B. Kempner fellowship.

* Corresponding author: Dr. W. M. Bujalowski, Department of Human Biological Chemistry & Genetics, The University of Texas Medical Branch at Galveston. Tel: (409) 772-5634. Fax: (409) 772−1790. E-mail: wbujalow@utmb.edu.

[1] Abbreviations: Tris, tris(hydroxymethyl)aminomethane; DTT, dithiothreitol; AMP−PNP, β,γ-imidoadenosine-5′-triphosphate.

10.1021/bi049378q CCC: $27.50
Published on Web 08/04/2004

of the PriA complexes with different ssDNA oligomers indicates that the ssDNA-binding site is located in the central part of the helicase molecule with the protein matrix extending over a distance of ~6 nucleotide residues on both sides of the ssDNA-binding site (*19*, *20*).

Although the importance of understanding the PriA protein interactions with the nucleic acid has been recognized, still little is known about the molecular details of these interactions, including quantitative aspects of the mechanism of the enzyme binding to different DNA conformational states, replication fork and the PAS structures, effect of solution conditions on the dynamics of interactions, and the structure of the complexes. Knowledge of the mechanism of binding and structure of the helicase−nucleic acid complex is a prerequisite to understand the enzyme functioning in DNA replication and recombination (*1*−*3*, *15*−*18*). Such knowledge is of fundamental importance for formulating any model of the enzyme translocation on the DNA, catalysis of DNA unwinding, as well as the functioning of the PriA helicase in the formation and translocation of the primosome.

In this paper, we report quantitative analyses of the kinetics of the PriA helicase interactions with a series of ssDNA oligomers using the fluorescence stopped-flow technique. To our knowledge, this is the first analysis of the dynamics of the PriA helicase−ssDNA interactions. The PriA helicase binds the ssDNA in a minimum three-step sequential reaction. The bimolecular step is very fast, without inducing significant conformational changes in the nucleic acid. Only the DNA-binding site that encompasses 6.3 ± 1 residues is directly involved in interactions with the DNA. The following intramolecular steps are independent of the length of the ssDNA and are accompanied by large changes in the DNA structure. Examination of the effect of solution conditions on the dynamics of the enzyme−ssDNA interactions indicates a very different nature of the formed intermediates and specific ion binding to the protein that stabilizes the helicase−nucleic acid complex. The sequential mechanism of the PriA binding to the ssDNA provides a very strong indication that the enzyme does not exist in a preequilibrium conformational transition prior to the nucleic acid binding.

MATERIALS AND METHODS

Reagents and Buffers. All chemicals were reagent grade. All solutions were made with distilled and deionized 18 MΩ (Milli-Q) water. The standard buffer, C, is 10 mM sodium cacodylate adjusted to pH 7.0 with HCl, 25% glycerol, 0.1 mM EDTA, and 1 mM DTT. The salt concentration in the buffer is indicated in the text.

Nucleic Acids. Oligomers $dA(pA)_7$, $dA(pA)_8$, $dA(pA)_{11}$, $dA(pA)_{15}$, $dA(pA)_{19}$, $dA(pA)_{23}$ were purchased from Midland Certified Reagents (Midland, Texas). Oligomers were at least >95% pure as judged by autoradiography of ^{32}P-labeled oligomers on polyacrylamide gels. The etheno derivatives of the oligomers were obtained by modification with chloroacetaldehyde (*21*−*25*). This modification goes to completion and provides a fluorescent derivative of the nucleic acid. The concentration of the etheno derivative of nucleic acids was determined using extinction coefficient 3700 cm^{-1} M^{-1} (nucleotide) at 257 nm (*21*−*25*).

PriA Protein. The *E. coli* PriA protein has been isolated and purified as we described before (*19*, *20*). The concentration of the protein was spectrophotometrically determined, with extinction coefficient $\epsilon_{280} = 1.06 \times 10^5$ cm^{-1} M^{-1} (monomer) determined using a method based on the Edelhoch's approach (*19*, *20*, *26*, *27*).

Stopped-Flow Kinetics. All fluorescence stopped-flow kinetics experiments were performed using the SX.18MV stopped-flow instrument (Applied Photophysics, Leatherhead, UK) as described before (*28*−*33*). The reactions were monitored following the fluorescence emission of the etheno derivative of ssDNA oligomers, with $\lambda_{ex} = 325$ nm, and the emission was monitored through the GG400 cutoff filter (Schott, PA). The excitation monochromator slits were at 1.5 mm (band-pass ≈ 7 nm). Four to twelve traces were collected and averaged for each sample. The relaxation times and amplitudes for each kinetic trace were determined using the nonlinear, least-squares software provide by the manufacturer, with the exponential function defined as

$$F(t) = F(\infty) + \sum_{i=1}^{n} A_i \exp(-\lambda_i t) \qquad (1)$$

where $F(t)$ is the fluorescence intensity at time t, $F(\infty)$ is the fluorescence intensity at time $t = \infty$, A_i is the amplitude corresponding to the ith relaxation process, λ_i is the time constant (reciprocal relaxation time) characterizing the ith relaxation process, and n is the number of relaxation processes. All further analyses of the data were performed using Mathematica (Wolfram, Urbana, IL) and KaleidaGraph (Synergy Software, PA).

Analysis of Kinetic Data. Analyses of the stopped-flow kinetic data have been performed using the matrix projection operator technique (*28*−*33*). This approach is particularly useful in the analyzing the amplitudes of the studied reactions and has been extensively described by us before (*28*−*33*).

RESULTS

Kinetics of PriA Helicase Binding to the ssDNA Substrate Within the Total PriA−ssDNA Binding Site. Dynamics of PriA−ssDNA 20-mer Interactions. Binding of the PriA helicase to etheno derivatives of the ssDNA is accompanied by a strong nucleic acid fluorescence increase (*19*, *20*). Such a large emission change provides an excellent signal to monitor the PriA−ssDNA kinetics and to perform high-resolution measurements of the mechanism of the helicase−ssDNA complex formation. Quantitative thermodynamic analyses showed that the total site-size of the PriA−ssDNA complex, i.e., the maximum number of nucleotide residues occluded by the PriA helicase in the complex, is 20 ± 3 residues per protein monomer, although the ssDNA binding site occludes, at most, ~8 nucleotide residues (*19*, *20*). Therefore, in the first set of experiments, we addressed the dynamics of the helicase interactions with the ssDNA within the total site-size of the formed complex, by examining the kinetics of the enzyme binding to the ssDNA 20-mer, $d\epsilon A(p\epsilon A)_{19}$.

The fluorescence stopped-flow kinetic trace of the ssDNA 20-mer, $d\epsilon A(p\epsilon A)_{19}$, after mixing 3×10^{-7} M nucleic acid with 7.3×10^{-6} M PriA (final concentrations) in buffer C (pH 7.0, 10 °C), containing 100 mM NaCl, is shown in Figure 1a. To increase the resolution, the plot is shown in

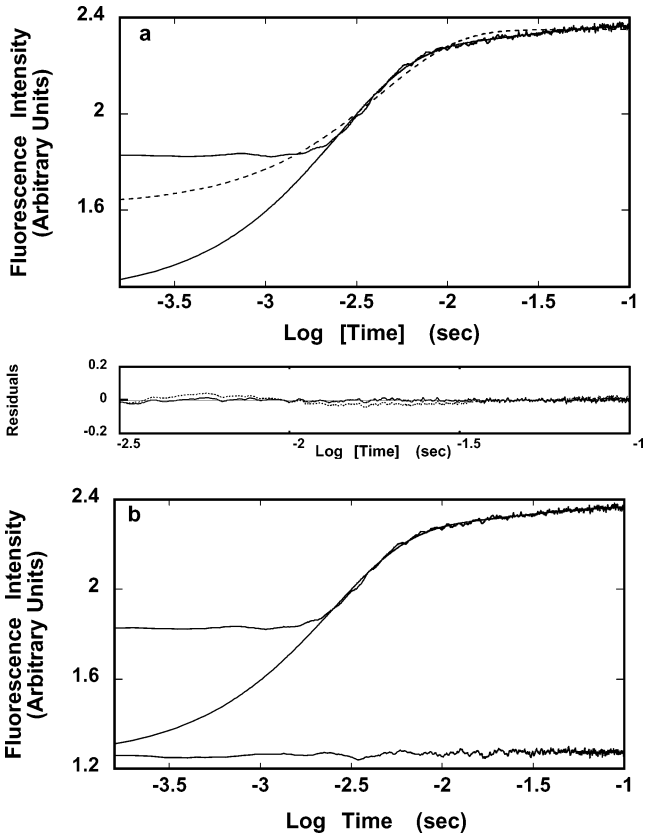

FIGURE 1: (a) The fluorescence stopped-flow kinetic trace, after mixing PriA helicase with the ssDNA 20-mer, dϵA(pϵA)$_{19}$ in buffer C (pH 7.0, 10 °C), containing 100 mM NaCl (λ = 325 nm, λ_{em} > 400 nm). The final concentrations of the helicase and the 20-mer are 7.3×10^{-6} and 3×10^{-7} M, respectively. The solid line is the two-exponential, nonlinear least-squares fit of the experimental curve, using eq 1. The dashed line is the nonlinear least-squares fit using the single-exponential function. The horizontal, initial part of the trace is the steady-state value of the fluorescence of the sample recorded 2 ms before the flow stopped. Lower panel shows the residuals for the fits using single-exponential and two-exponential functions. (b) The same fluorescence stopped-flow trace, as in panel a, together with the zero line trace (lower trace), which is obtained after mixing the nucleic acid, at the same concentration as used with the protein, but only with the buffer. The solid line is the same two-exponential, nonlinear least-squares fit of the experimental curve as shown in panel a.

logarithmic scale with respect to time. The initial horizontal part of the trace corresponds to the steady-state fluorescence intensity of the sample, recorded for ~2 ms, before the flow stops (*33*). The solid line in Figure 1a is a nonlinear, least-squares fit of the experimental curve using a two-exponential fit as defined by eq 1. The included single-exponential function does not provide an adequate description of the observed kinetics (dashed line). Using larger number of exponents in the fitting function (eq 1) does not improve the statistics of the fit (data not shown).

The stopped-flow kinetic trace, together with the trace corresponding to the ssDNA oligomer alone, at the same concentration of the nucleic acid as used with the protein, but only mixed with the background buffer (zero line), is shown in Figure 1b. As we pointed out before, comparison between the determined relaxation amplitudes and the total amplitude of the kinetic trace, at several enzyme concentrations, is crucial in establishing that the resolved relaxation processes account for the total observed signal (*30*, *31*). The two-exponential fit provides an excellent description of the observed kinetic process, yielding the sum of amplitudes that is the same as the observed total amplitude of the overall, relaxation process. Because this behavior is observed at all studied enzyme concentrations, i.e., no signal change is lost in the instrumental dead time, the simplest interpretation would be that the enzyme binding to the ssDNA is a two-step process (*28*, *29*, *34*, *35*). However, the behavior of the relaxation times and amplitudes shows that the binding is characterized by a more complex mechanism (*30*, *31*).

The dependence of the reciprocal relaxation times, $1/\tau_1$ and $1/\tau_2$, upon the total concentration of PriA is shown in Figure 2a,b. The functional dependence of $1/\tau_1$ upon [PriA] shows a typical nonlinear, hyperbolic dependence upon [PriA], in the examined enzyme concentration range. Thus, it is evident that the shortest observed relaxation time does not describe the bimolecular reaction, where a strictly linear dependence upon the enzyme concentration is expected (*28*, *29*, *34*, *35*). The nonlinear character of the plot in Figure 2a indicates that τ_1 characterizes an intramolecular transition. The values of $1/\tau_2$ are independent of the helicase concentration, clearly indicating that this relaxation time characterizes another intramolecular transition of the protein−ssDNA complex. Therefore, the simplest mechanism that can describe the observed dependence of the relaxation times upon the PriA concentration is a sequential reaction in which the PriA helicase binds the ssDNA in a very fast bimolecular step, followed by two first-order transitions of the formed protein−ssDNA complex, as described by Scheme 1.

Figure 2c shows the dependence of the normalized, individual amplitudes, A_1 and A_2, of the two observed relaxation steps upon the logarithm of PriA concentration. The amplitude of the first relaxation step, A_1, dominates the relaxation process over the entire examined range of [PriA]. Also, its values slightly increase with increasing concentrations of the helicase. Values of the amplitude, A_2, are significantly lower than A_1 and slightly decrease with the increasing of the [enzyme]. As mentioned above, the amplitude of the bimolecular step is undetectable, i.e., its values must be below ~1% of the total signal, in the examined protein concentration range. The observed behavior of the resolved individual amplitudes as functions of the PriA concentration is in excellent agreement with the proposed mechanism defined by Scheme 1 (see below).

The analysis of the relaxation data in Figure 2a,b,c is initiated by numerical nonlinear, least-squares fitting of the individual relaxation times. Because the rate of the bimolecular step is very fast, the relaxation time characterizing the first normal mode of the reaction is beyond the resolution of the stopped-flow technique. On the other hand, because of the fast rate, the step equilibrates before the transition to the next intermediate takes place, allowing us to use the overall partial equilibrium constant, $K_I = k_I/k_{-1}$, as a fitting parameter (Scheme 1). Notice, the overall rate constant k_I differs from k_1 by a statistical factor resulting from the presence of potential binding sites on the DNA (see below). The analyses are facilitated by the fact that we also know the value of the overall macroscopic binding constant, K_N, for the enzyme binding to the ssDNA 20-mer. The value of K_{20} is $(4.9 \pm 0.6) \times 10^5$ M^{-1} and has been independently obtained in the same solution conditions by the equilibrium fluorescence titration method (*19*, *20*). The macroscopic

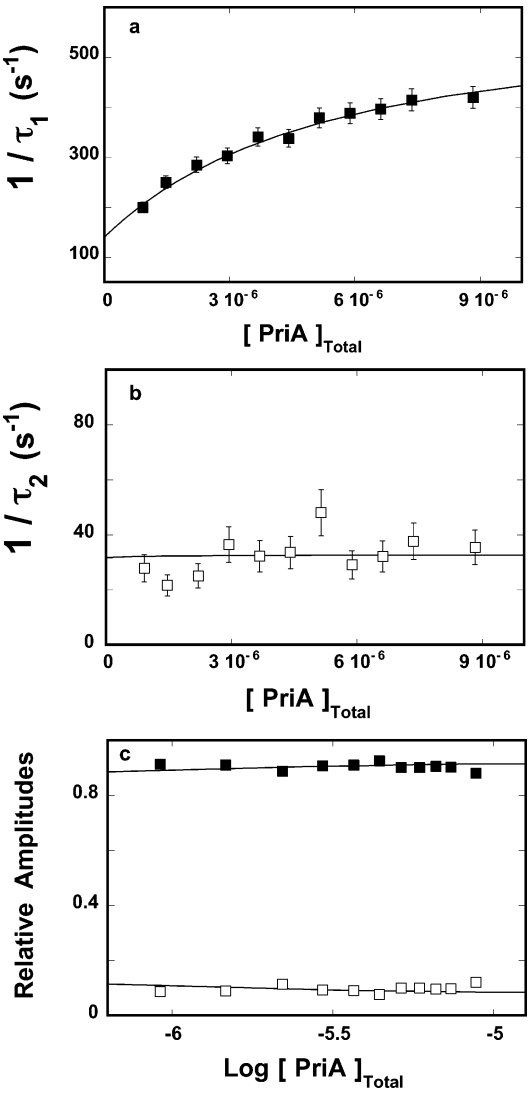

FIGURE 2: (a) The dependence of the reciprocal relaxation time, $1/\tau_1$, for the binding of the PriA helicase to the ssDNA 20-mer, dϵA(pϵA)$_{19}$, in buffer C (pH 7.0, 10 °C), containing 100 mM NaCl, upon the total concentration of the enzyme. The solid line is the nonlinear least-squares fit according to the three-step sequential mechanism, defined by Scheme 1, with the overall partial equilibrium constant $K_I = 2 \times 10^5$ M^{-1} and the rate constants: $k_2 = 230$ s^{-1}, $k_{-2} = 140$ s^{-1}, $k_3 = 1$ s^{-1}, and $k_{-3} = 32$ s^{-1} (details in text). The error bars are standard deviations obtained from 3 to 4 independent experiments. (b) The dependence of the reciprocal relaxation time, $1/\tau_2$, for the binding of the PriA helicase to the ssDNA 20-mer, dϵA(pϵA)$_{19}$, in buffer C (pH 7.0, 10 °C), containing 100 mM NaCl, upon the total concentration of the enzyme. The solid lines is the nonlinear least-squares fit according to the three-step sequential mechanism, defined by Scheme 1, with the same overall partial equilibrium constant, K_I, and the rate constants, k_2, k_{-2}, k_3, and k_{-3}, as in panel a. (c) The dependence of the individual relaxation amplitudes, A_1, and A_2, for the binding of the PriA helicase to the 20-mer, dϵA(pϵA)$_{19}$, in buffer C (pH 7.0, 10 °C), containing 100 mM NaCl, upon the total concentration of the enzyme. The solid lines are nonlinear least-squares fits according to the three-step sequential mechanism, defined by Scheme 1, with the relative fluorescence intensities $F_2 = 1.02$, $F_3 = 2.75$, and $F_4 = 7$. The maximum fluorescence increase of the nucleic acid is taken from the equilibrium fluorescence titration in the same solution conditions as $\Delta F_{max} = 2.2$ (Table 1). The rate constants are the same as in panel a. A_1 (■), A_2 (□).

binding constant, K_{20}, is related to the overall bimolecular partial equilibrium constant K_I, and partial equilibrium

Scheme 1

$$\mathrm{PriA + ssDNA} \underset{k_{-1}}{\overset{k_1}{\leftrightarrow}} (P)_1 \underset{k_{-2}}{\overset{k_2}{\leftrightarrow}} (P)_2 \underset{k_{-3}}{\overset{k_3}{\leftrightarrow}} (P)_3$$

constants characterizing the intramolecular transitions by

$$K_{20} = K_I(1 + K_2 + K_2K_3) \quad (2)$$

where $K_2 = k_2/k_{-2}$ and $K_3 = k_3/k_{-3}$ (see below). The above relationship reduces the number of independent parameters in fitting the relaxation times to four. Subsequently, the obtained rate constants are used as starting values in the fitting of the individual amplitudes and extract relative molar fluorescence parameters, i.e., to assess the conformational state of the helicase−nucleic acid complex in each intermediate. This is accomplished using the matrix projection operator technique (*28*−*33*). This part of the analysis uses the value of the maximum relative increase of the ssDNA fluorescence accompanying the complex formation, $\Delta F_{max} = 2.2 \pm 0.1$, that is known from independent equilibrium fluorescence titrations (*19*, *20*). The ΔF_{max} parameter can be analytically expressed as (*28*−*33*)

$$\Delta F_{max} = \frac{\Delta F_2}{1 + K_2 + K_2K_3} + \frac{K_2\Delta F_3}{1 + K_2 + K_2K_3} + \frac{K_2K_3\Delta F_4}{1 + K_2 + K_2K_3} \quad (3)$$

where $\Delta F_2 = (F_2 - F_1)/F_1$, $\Delta F_3 = (F_3 - F_1)/F_1$, and $\Delta F_4 = (F_4 - F_1)/F_1$ are fractional fluorescence intensities of each intermediate in the formation of the complex, relative to the molar fluorescence intensity of the free DNA oligomer, F_1. Contrary to the ΔF_i's, the fluorescence parameters, F_2, F_3, and F_4, are relative molar fluorescence intensities, but not fractional intensities, with respect to the free nucleic acid fluorescence. Expression 3 provides an additional relationship among the fitted parameters, thus decreasing the number of independent variables. The refinement of the values of rate constants and molar fluorescence parameters is accomplished by global fitting of all relaxation times and amplitudes. The solid lines in Figure 2a,b,c are nonlinear least-squares fits of the relaxation times and amplitudes, according to the mechanism defined by Scheme 1, using a single set of rate and spectroscopic parameters. The obtained rate constants and relative molar fluorescence intensities are included in Table 1.

Comparison between the value of the overall partial equilibrium constant, $K_I = (2 \pm 0.5) \times 10^5$ M^{-1}, with the overall equilibrium constant $K_{20} = (4.9 \pm 0.6) \times 10^5$ M^{-1} indicates that the fast, bimolecular step provides the major part of the free energy of binding, $\Delta G°$, of the enzyme to the ssDNA. Nevertheless, very low, if any, fluorescence change of the nucleic acid in this step strongly suggests the lack of any significant conformational changes of the nucleic acid structure accompanying the formation of the $(P)_1$ intermediate (see below). The transition to the second intermediate, $(P)_2$, is also a fast process with the forward rate constant, $k_2 = 230 \pm 40$ s^{-1} (Table 1). However, contrary to the $(P)_1$, there is a large molar fluorescence increase ($F_3 = 2.75 \pm 0.15$) accompanying the formation of $(P)_2$, an indication of a large conformational change of the DNA, as compared to the free nucleic acid, occurring in the complex

Table 1: Kinetic, Thermodynamic, and Spectroscopic Parameters for the PriA Helicase Binding to ssDNA Oligomers, Differing in the Number of Nucleotide Residues, *N*, in Buffer C (pH 7.0, 10 °C), Containing 100 mM NaCl

ssDNA oligomer *N*	K_N (M^{-1})	ΔF_{max}[a]	K_1 (M^{-1})	k_2 (s^{-1})	k_{-2} (s^{-1})	k_3[b] (s^{-1})	k_{-3} (s^{-1})	K_2	K_3	K_{ov} (M^{-1})	F_2[c]	F_3[c]	F_4[c]
8	$(8.5 \pm 1) \times 10^4$	1.5 ± 0.2	$(3.4 \pm 0.8) \times 10^4$	240 ± 40	160 ± 30	1	37 ± 8	1.50 ± 0.5	0.027 ± 0.01	$(8.6 \pm 2.5) \times 10^4$	1.02 ± 0.08	2 ± 0.1	4.5 ± 0.3
12	$(3.2 \pm 0.4) \times 10^5$	1.71 ± 0.1	$(1.0 \pm 0.2) \times 10^5$	230 ± 40	145 ± 30	1	35 ± 8	1.6 ± 0.6	0.028 ± 0.01	$(2.6 \pm 0.8) \times 10^5$	1.02 ± 0.08	2.1 ± 0.1	4 ± 0.3
16	$(3.3 \pm 0.4) \times 10^5$	1.7 ± 0.1	$(1.4 \pm 0.3) \times 10^5$	230 ± 40	165 ± 40	1	30 ± 7	1.4 ± 0.5	0.033 ± 0.015	$(3.4 \pm 1.1) \times 10^5$	1.02 ± 0.08	2.1 ± 0.1	4.3 ± 0.3
20	$(4.9 \pm 0.6) \times 10^5$	2.2 ± 0.3	$(2.0 \pm 0.5) \times 10^5$	230 ± 40	140 ± 30	1	32 ± 7	1.6 ± 0.6	0.031 ± 0.015	$(5.4 \pm 1.6) \times 10^5$	1.02 ± 0.08	2.75 ± 0.15	7 ± 0.8
24	$(3.7 \pm 0.5) \times 10^5$	2.5 ± 0.3	$(2.6 \pm 0.7) \times 10^5$	220 ± 40	160 ± 40	1	45 ± 8	1.4 ± 0.5	0.044 ± 0.02	$(6.3 \pm 2.1) \times 10^5$	1.02 ± 0.08	3.3 ± 0.2	7.7 ± 0.8

[a] Determined in independent fluorescence titrations (*19*, *20*). [b] Maximum estimated value. [c] Values relative to the fluorescence, $F_1 = 1$ of the free $d\epsilon A(p\epsilon A)_N$ (details in text).

(see Discussion). Nevertheless, the value of $k_{-2} = 140 \pm 30$ s^{-1} indicates that the enzyme can quickly return to the $(P)_1$ intermediate. On the other hand, the transition to $(P)_3$ is much slower, with the forward rate constant, k_3, being approximately more than 2 orders of magnitude lower than k_2. Also, the $(P)_2 \leftrightarrow (P)_3$ transition is accompanied by a dramatically large increase of the nucleic acid fluorescence (Table 1). The obtained rate constants for the second and third step provide partial equilibrium constants $K_2 = 1.6 \pm 0.6$, and $K_3 \approx 0.031$. Thus, only the second step contributes additional favorable contribution to the $\Delta G°$, while the $(P)_2 \leftrightarrow (P)_3$ transition is energetically unfavorable.

Dependence of the Kinetics of PriA−ssDNA Interactions Upon the Length of the ssDNA Substrate. Thermodynamic studies of PriA interactions with the ssDNA showed that, although the total site-size of the PriA−ssDNA complex is 20 ± 3 nucleotide residues, the DNA-binding site of the enzyme occludes only 8 ± 1 nucleotides (*19*, *20*). To obtain further insight into the dynamics of the helicase−ssDNA interactions, we performed analogous stopped-flow kinetic studies, as described above, with a series of ssDNA oligomers of different lengths. The shortest oligomer, $d\epsilon A(p\epsilon A)_7$, contains eight residues, i.e., it corresponds to the determined maximum size of the ssDNA-binding site. The longest oligomer, $d\epsilon A(p\epsilon A)_{23}$, is three times longer than the ssDNA-binding site but can still accept only one PriA molecule. The experiments have been performed in the same solution conditions, i.e., buffer C (pH 7.0, 10 °C), containing 100 mM NaCl.

For all examined ssDNAs, the experimental kinetic traces required a two-exponential fit and the amplitudes of the two resolved relaxation processes account for the total amplitude of the kinetic traces (data not shown). The reciprocal relaxation time, $1/\tau_1$, for the association of PriA with various ssDNA oligomers as a function of the total PriA concentration, are shown in Figure 3a. There are two key aspects of these data. First, the kinetic mechanism is independent of the length of the ssDNA. Therefore, the association of PriA with all examined ssDNA oligomers is described by the same mechanism as depicted by Scheme 1. With the increasing length of the ssDNA oligomer, the values of $1/\tau_1$ show a more and more pronounced hyperbolic dependence upon [PriA] and higher plateau at saturating concentrations of the helicase (Figure 3a). Second, the plots intercept the reciprocal relaxation time axis at a very similar point, indicating that the values of k_{-2} are very close for all oligomers (*34*, *35*).

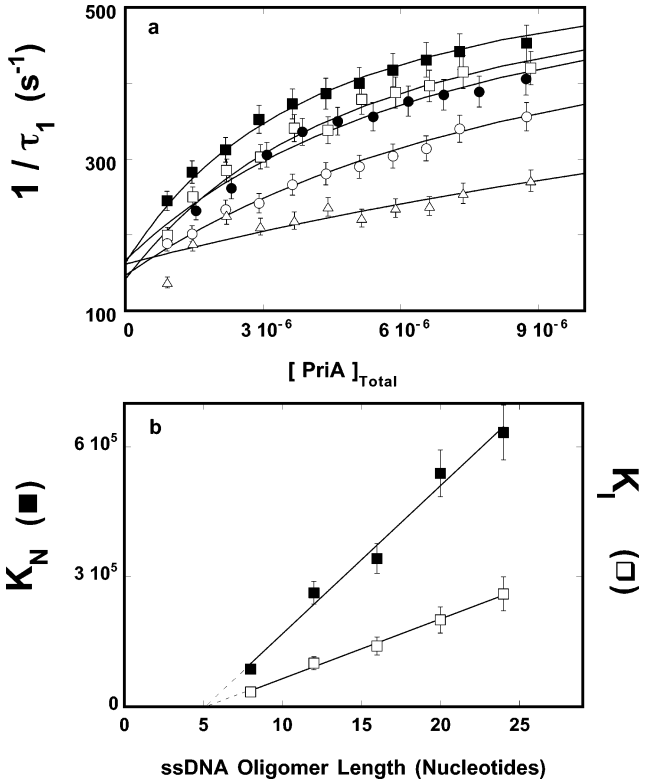

FIGURE 3: (a) The dependence of the reciprocal relaxation time, $1/\tau_1$, for the binding of the PriA helicase to the ssDNA oligomers, differing in the number of nucleotide residues, in buffer C (pH 7.0, 10 °C), containing 100 mM NaCl, upon the total concentration of the enzyme. The concentration of the nucleic acids is 3×10^{-7} M (oligomer). The solid lines are nonlinear least-squares fits according to the three-step sequential mechanism, defined by Scheme 1, with partial equilibrium constants, K_I, and rate constants included in Table 1; (△) 8-mer, $d\epsilon A(p\epsilon A)_7$, (○) 12-mer, $d\epsilon A(p\epsilon A)_{11}$, (●) 16-mer, $d\epsilon A(p\epsilon A)_{15}$, (□) 20-mer, $d\epsilon A(p\epsilon A)_{19}$, (■) 24-mer, $d\epsilon A(p\epsilon A)_{23}$, The error bars are standard deviations obtained from 3 to 4 independent experiments. (b) The dependence of the overall equilibrium constant, K_N (■), and overall partial equilibrium constant, K_1 (□), characterizing the bimolecular step (Scheme 1), for PriA binding to ssDNA oligomers with different number of nucleotide residues, upon the length of the ssDNA oligomer (nucleotides). The solid lines are the linear least-squares fits of the plots according to eqs 4c and 5b. The dashed lines are extrapolations of the plots to zero value of the corresponding equilibrium constant.

Contrary to $1/\tau_1$, the values of $1/\tau_2$ exhibit little dependence upon the length of ssDNA oligomers, i.e., the $(P)_2 \leftrightarrow (P)_3$ transition is only slightly affected by the length of the ssDNA (data not shown) (Table 1).

Table 2: Kinetic and Thermodynamic Parameters Characterizing the Binding of the PriA Helicase to the ssDNA Oligomer dϵA(pϵA)$_{15}$, in Buffer C (pH 7.0, 10 °C), Containing Different Concentrations of NaCl

[NaCl] mM	K_{16}[a] (M^{-1})	ΔF_{max}[a]	K_1 (M^{-1})	k_2 (s^{-1})	k_{-2} (s^{-1})	k_3[b] (s^{-1})	k_{-3} (s^{-1})	K_2	K_3	K_{16} (M^{-1})	F_2[c]	F_2[c]	F_4[c]
75	$(7.5 \pm 0.8) \times 10^5$	2.2 ± 0.1	$(4.2 \pm 1) \times 10^5$)	250 ± 40	250 ± 40	1	60 ± 15	1 ± 0.3	0.017 ± 0.008	$(8.5 \pm 2.8) \times 10^5$	1.02 ± 0.03	3.4 ± 0.2	12 ± 1
88	$(4.7 \pm 0.5) \times 10^5$	1.9 ± 0.1	$(2.2 \pm 0.5) \times 10^5$	260 ± 40	230 ± 40	1	45 ± 8	1.1 ± 0.3	0.022 ± 0.01	$(4.7 \pm 1.3) \times 10^5$	1.02 ± 0.03	2.8 ± 0.2	7 ± 0.8
100	$(3.3 \pm 0.4) \times 10^5$	1.7 ± 0.1	$(1.4 \pm 0.3) \times 10^5$	280 ± 50	210 ± 35	1	40 ± 8	1.3 ± 0.4	0.025 ± 0.012	$(3.3 \pm 1.1) \times 10^5$	1.02 ± 0.03	2.2 ± 0.2	4.5 ± 0.5
112	$(2.4 \pm 0.3) \times 10^5$	1.4 ± 0.1	$(7.0 \pm 1.5) \times 10^4$	400 ± 80	160 ± 30	1	40 ± 8	2.5 ± 1	0.025 ± 0.012	$(2.5 \pm 0.8) \times 10^5$	1.02 ± 0.03	1.7 ± 0.2	3.6 ± 0.3
125	$(1.8 \pm 0.2) \times 10^5$	1.2 ± 0.1	$(4.5 \pm 1) \times 10^5$	430 ± 80	150 ± 30	1	50 ± 8	2.9 ± 1	0.020 ± 0.01	$(1.8 \pm 0.6) \times 10^5$	1.02 ± 0.03	1.4 ± 0.15	3.2 ± 0.3
150	$(1.1 \pm 0.15) \times 10^5$	1.1 ± 0.1	$(2.6 \pm 0.5) \times 10^5$	500 ± 80	140 ± 30	1	30 ± 7	3.6 ± 1.1	0.033 ± 0.015	$(1.2 \pm 0.4) \times 10^5$	1.02 ± 0.03	1.3 ± 0.15	2 ± 0.2

[a] Determined in independent fluorescence titrations (*19*, *20*). [b] Maximum estimated value. [c] Values relative to the fluorescence, $F_1 = 1$ of the free dϵA(pϵA$_{15}$) (details in text).

The analyses of relaxation times and amplitudes have been performed, using the same strategy as described above. The obtained values of all kinetic and spectroscopic parameters are included in Table 1. It is evident that the increasing hyperbolic dependence of $1/\tau_1$ results from the increasing values of the overall partial equilibrium constant, K_I, characterizing the bimolecular step in the enzyme binding to the longer ssDNA oligomers, and not from the increased values of the rate constant, k_2. In fact, both k_2 and k_{-2} are, within the experimental accuracy, unaffected by the length of the nucleic acid (Table 1). The same is true for k_3 and k_{-3}. Thus, the entire effect of the different length of the ssDNA oligomers on the dynamics of the enzyme interactions with the ssDNA is confined to the bimolecular step of the reaction (see Discussion).

Figure 3b shows the overall equilibrium constant K_N, and the overall partial equilibrium constant K_I (Table 1), for PriA binding to ssDNA oligomers with a different number of nucleotide residues, as functions of the ssDNA oligomer length. A very characteristic feature of these plots is that they are strictly linear, although their slopes are different. Moreover, extrapolations of the plots to zero value of the corresponding equilibrium constant, intercept the DNA length axis at very similar points (Figure 3b). Such strictly linear behavior of both K_N and K_I as a function of the length of ssDNA oligomers can quantitatively be understood in terms of the existence of several potential binding sites on the ssDNA oligomers, resulting from the fact that the size of the DNA-binding site of the PriA helicase, n, is significantly smaller than the total site-size of the enzyme−ssDNA complex, $n_t = 20 \pm 3$ (*19*, *20*).

In terms of the potential binding sites and partial equilibrium constants, the overall binding constant, K_N, for the helicase binding to the ssDNA oligomer containing N nucleotide residues, is analytically defined as

$$K_N = K_I(1 + K_2 + K_2K_3) \tag{4a}$$

$$K_N = (N - n + 1)K_1(1 + K_2 + K_2K_3) \tag{4b}$$

and

$$K_N = NK_1(1 + K_2 + K_2K_3) - (n - 1)K_1(1 + K_2 + K_2K_3) \tag{4c}$$

where N is the total length of the ssDNA oligomer in nucleotides and K_1 is the partial equilibrium constant, characterizing the bimolecular step, i.e., $K_1 = k_1/k_{-1}$. Thus, it is evident that K_N must be a linear function of N with the slope $\partial K_N/\partial N = K_1(1 + K_2 + K_2K_3)$ (Figure 3b). Moreover, K_N is equal to 0 for $N = n - 1$, i.e., no binding will be observed for the ssDNA oligomer shorter by one residue than the size of the DNA-binding site. Thus, the plot of K_N as a function of the nucleic acid length will intercept the N axis at the value of $N = n - 1$. Analogously, the overall partial equilibrium constant, K_I, characterizing the bimolecular step is defined in terms of potential binding sites and partial equilibrium constant, K_1, as

$$K_I = (N - n + 1)K_1 \tag{5a}$$

and

$$K_I = NK_1 - (n - 1)K_1 \tag{5b}$$

Thus, the plot of K_I as a function of N is linear with respect to N, with the slope $\partial K_I/\partial N = K_1$. The value of $\partial K_I/\partial N$ is lower than $\partial K_N/\partial N$ by a factor, $(1 + K_2 + K_2K_3)$. The plot intercepts the nucleic acid axis at $N = n - 1$. Extrapolations of both plots in Figure 3b provide $n = 6.3 \pm 1$ as compared to the maximum value of $n = 8 \pm 1$, obtained in independent thermodynamic analyses (*19*, *20*; see Discussion).

Salt Dependence of the Kinetics of PriA−ssDNA Interactions. Equilibrium binding studies indicate that the binding of PriA to the ssDNA is significantly affected by the salt concentration in solution (*20*). As the salt concentration increases, the overall affinity of the enzyme for the nucleic acid decreases. Further insight into the nature of the observed intermediates can be obtained by examining the salt effect on the kinetics of the binding of the helicase to the ssDNA. The salt effect on the kinetics of PriA helicase−ssDNA interactions has been addressed using the ssDNA 16-mer, dϵA(pϵA)$_{15}$. The selection of the oligomer was dictated by the fact that it encompasses most of the total site-size of the enzyme−ssDNA complex and allows us to perform experiments over a large protein concentration range, in various solution conditions, avoiding the precipitation of the sample (*19*, *20*). The stopped-flow experiments have been performed in buffer C (pH 7.0, 10 °C) containing different NaCl concentrations. Analyses of relaxation curves have been performed as described above, and the obtained kinetic and thermodynamic parameters are included in Table 2.

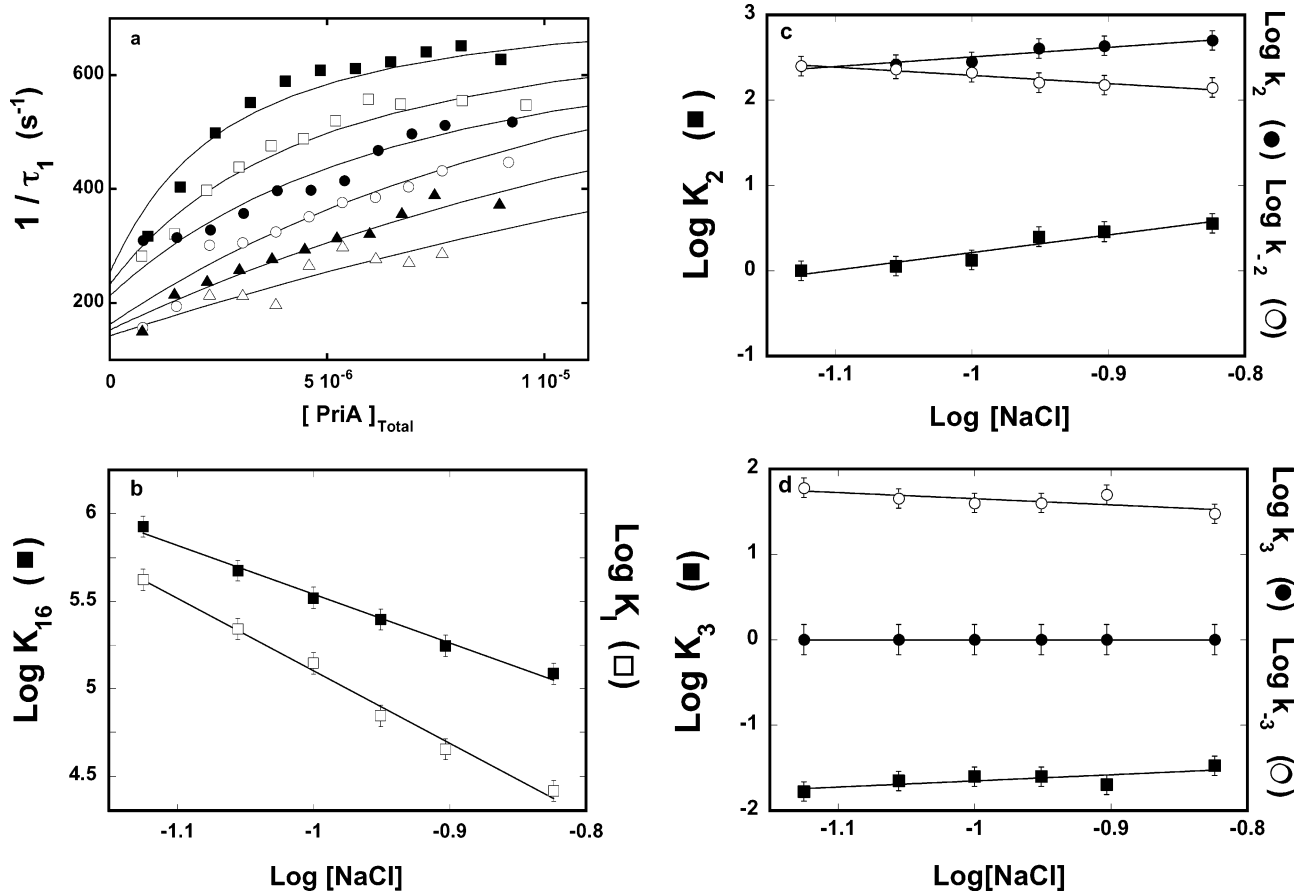

FIGURE 4: (a) The dependence of the reciprocal relaxation time, $1/\tau_1$, for the binding of the PriA helicase to the ssDNA 16-mer, dϵA-(pϵA)$_{15}$, in buffer C (pH 7.0, 10 °C), containing different NaCl concentrations, upon the total concentration of the enzyme. The concentration of the 16-mer is 3×10^{-7} M (oligomer). The solid lines are nonlinear least-squares fits according to the three-step sequential mechanism, defined by Scheme 1, with partial equilibrium constants, K_I, and rate constants included in Table 2. The concentration of NaCl is (■) 75 mM, (□) 88 mM, (●) 100 mM, (○) 112 mM, (▲) 125 mM, and (△) 150 mM. (b) The dependence of the logarithm of the overall partial equilibrium constant, K_{16} (■) and overall partial equilibrium constant, K_1 (□), characterizing the bimolecular step for the PriA helicase binding to the ssDNA 16-mer, dϵA(pϵA)$_{15}$, (Scheme 1) upon the log[NaCl] (log−log plots). The plots are characterized by the slopes $\partial \log K_{16}/\partial \log[\mathrm{NaCl}] = -2.8 \pm 0.3$, and $\partial \log K_1/\partial \log[\mathrm{NaCl}] = -4.2 \pm 0.3$, respectively. (c) The dependence of the logarithm of the partial equilibrium constants, K_2 (■) and rate constants, k_2 (●) and k_{-2} (○), (Scheme 1) characterizing the first intramolecular step $(P)_1 \leftrightarrow (P)_2$, in the binding of the PriA helicase to the ssDNA 16-mer, dϵA(pϵA)$_{15}$, upon the log[NaCl]. The plots are characterized by the slopes $\partial \log K_2/\partial \log[\mathrm{NaCl}] = 2.1 \pm 0.3$, $\partial \log k_2/\partial \log[\mathrm{NaCl}] = 1.1 \pm 0.25$, $\partial \log k_{-2}/\partial \log[\mathrm{NaCl}] = -0.9 \pm 0.25$. (d) The dependence of the logarithm of the partial equilibrium constants, K_3 (■) and rate constants, k_3 (●) and k_{-3} (○), (Scheme 1) characterizing the second intramolecular step $(P)_2 \leftrightarrow (P)_3$, in the binding of the PriA helicase to the ssDNA 16-mer, dϵA(pϵA)$_{15}$, upon the log[NaCl]. The plots are characterized by the slopes $\partial \log K_3/\partial \log[\mathrm{NaCl}] = 0.7 \pm 0.2$, $\partial \log k_3/\partial \log[\mathrm{NaCl}] \approx 0$, $\partial \log k_{-3}/\partial \log[\mathrm{NaCl}] = -0.7 \pm 0.25$.

The dependence of the reciprocal relaxation time, $1/\tau_1$, upon [PriA], at different NaCl concentrations, is shown in Figure 4a. The hyperbolic character of the plot decreases at higher salt concentrations, indicating that the overall partial equilibrium constant, K_I, decreases with the increasing of [NaCl]. Moreover, the intercept at $[\mathrm{PriA}]_{\mathrm{Total}} = 0$ decreases, i.e., the values of k_{-2} is lower at higher salt concentrations. A much less pronounced effect of the increasing [NaCl] is observed in the case of the reciprocal relaxation time $1/\tau_2$ (data not shown). In the case of the bimolecular step, only the overall partial equilibrium constant, K_I, is available from stopped-flow experiments (see above). The dependence of the logarithm of K_I upon the logarithm of [NaCl] (log−log plot) is shown in Figure 4b (*36*, *37*). The plot is linear in the examined salt concentration range and the slope of the plot $\partial \log K_1/\partial \log[\mathrm{NaCl}] = -4.2 \pm 0.3$ indicates that the release of ~4 ions accompanies the initial association of the protein with the nucleic acid (*36*, *37*). The dependence of the logarithm of the overall equilibrium constant, K_{16} upon the logarithm of [NaCl] is also included in Figure 4b. The slope is $\partial \log K_{16}/\partial \log[\mathrm{NaCl}] = -2.8 \pm 0.3$. Thus, the number of ions released in the bimolecular step is larger than the net number of ions released in the overall binding process. However, unlike the ssDNA length dependence discussed above, the value of K_2, characterizing the formation of the second intermediate in PriA binding to the ssDNA, $(P)_2$, shows a significant dependence upon salt concentration. The log−log plot for the partial equilibrium constant, K_2, is shown in Figure 4c. Contrary to dependence of K_I upon [NaCl], the plot is characterized by the positive slope $\partial \log K_2/\partial \log[\mathrm{NaCl}] = 2.1 \pm 0.3$, indicating that instead of release, a net uptake of ~2 ions accompanies the formation of the $(P)_2$ intermediate. The dependences of the logarithm of the rate constants, k_2 and k_{-2}, upon the logarithm of [NaCl] are also included in Figure 4c. The slopes are $\partial \log k_2/\partial \log[\mathrm{NaCl}] = 1.1 \pm 0.25$ and $\partial \log k_{-2}/\partial \log[\mathrm{NaCl}] = -0.95 \pm 0.25$. Thus, the net uptake of ~2 ions in the formation of the $(P)_2$ intermediate results from the net uptake of an ~1 ion in both, the formation of the transition state and its transformation from $(P)_2$.

Notice, the formation of the $(P)_2$ intermediate becomes significantly energetically favorable at elevated salt concentrations due to the increasing values of the k_2 and decreasing values of k_{-2} (see Discussion). The dependences of logarithms of K_3 and the rate constants, k_3 and k_{-3}, characterizing the transition $(P)_2 \leftrightarrow (P)_3$ transition, upon the logarithm of [NaCl] are shown in Figure 4d. The slopes of the log−log plots are $\partial \log K_3/\partial \log[NaCl] = 0.7 \pm 0.2$, $\partial \log k_3/\partial \log[NaCl] \approx 0$, and $\partial \log k_{-3}/\partial \log[NaCl] = -0.7 \pm 0.25$. Therefore, similar to the $(P)_1 \leftrightarrow (P)_2$ transition, formation of the $(P)_3$ intermediate is accompanied by net ion uptake occurring in the formation of the corresponding transition state from the final $(P)_3$ complex. Comparison of the relative molar fluorescence intensities for $d\epsilon A(p\epsilon A)_{15}$ binding to the PriA helicase, obtained at different salt concentrations, indicates that the value of F_2 that characterizes the $(P)_1$ intermediate is not affected by the increasing salt concentration in solution (Table 2). However, there is a clear effect of the increasing salt concentration on F_3 and, particularly, on F_4. In the examined salt concentration range, the value of F_2 decreases from 3.4 ± 0.2 to 1.3 ± 0.15 while F_4 decreases from 12 ± 1 to 2 ± 0.2. It is evident that increased salt concentration dramatically affects conformational changes in the ssDNA induced by the PriA helicase.

Very different values of the net ion release accompanying individual reaction steps clearly indicate that the overall net ion release, $m = \partial \log K_{16}/\partial \log[NaCl] = -2.8 \pm 0.3$, is not a simple sum of the ion release in partial reactions (*30*, *31*). For the considered mechanism of PriA binding to the ssDNA, defined by Scheme 1, the value of the overall equilibrium constant, K_N, is analytically related to the partial equilibrium constants, in terms of the potential binding sites, by eq 4b. The derivative of the logarithm of K_N, with respect to the logarithm of [NaCl], is then

$$m = \frac{\partial \log K_{16}}{\partial \log[NaCl]} = m_I + \left[\frac{K_2 + K_2K_3}{1 + K_2 + K_2K_3}\right]m_2 + \left[\frac{K_2K_3}{1 + K_2 + K_2K_3}\right]m_3 \quad (6)$$

where $m_I = \partial \log K_I/\partial \log[NaCl]$, $m_2 = \partial \log K_2/\partial \log[NaCl]$, and $m_3 = \partial \log K_3/\partial \log[NaCl]$ are the numbers of ions released in the partial reaction for the formation of the $(P)_1$, $(P)_2$, and $(P)_3$ intermediates. Taking the experimental values of $m_I = -4.2$, $m_2 = 2.1$, and $m_3 = 0.7$, and partial equilibrium constants determined at a reference salt concentration of 100 mM NaCl, one obtains $m = \partial \log K_{16}/\partial \log[NaCl] = -2.95$, which is similar to the experimentally obtained net number of ions released, $m = -2.8 \pm 0.3$ (see above).

Glycerol Effect on the Kinetics of PriA−ssDNA Interactions. The PriA helicase requires an elevated glycerol concentration in solution to preserve prolonged protein stability (*19*, *20*). Fluorescence titrations of the ssDNA 16-mer, $d\epsilon A(p\epsilon A)_{15}$, with the PriA helicase, in buffer C (pH 7.0, 10 °C), containing 100 mM NaCl and different glycerol concentrations, are shown in Figure 5a. There is a decrease of the maximum fluorescence increase at saturation, ΔF_{max}, from 1.9 ± 0.1 at 20% glycerol to 1.4 ± 0.1 at 35% glycerol. These values of ΔF_{max} are ∼30% lower than observed previously (*19*, *20*). We found that different preparations of the PriA helicase slightly differ in the observed ΔF_{max}, although the values of the binding constants are unaffected (*19*). Therefore, all comparative studies, as described in this work, have always been performed with a single preparation of the protein. The solid lines in Figure 5a are computer fits to the single-site binding model with two fitting parameters, binding constant, K_{16}, and the maximum relative fluorescence increase, ΔF_{max} as defined by

$$\Delta F = \Delta F_{max}\left(\frac{K_{16}P_F}{1 + K_{16}P_F}\right) \quad (7)$$

where K_{16} is the overall binding constant for PriA helicase for the ssDNA 16-mer, and P_F is the free PriA concentration. The obtained binding parameters are included in Table 3.

Glycerol is a neutral compound and its concentrations used in titrations shown in Figure 5a are comparable to the water concentration in the sample. The simplest interpretation of the observed glycerol effect on the PriA binding to the ssDNA is that it reflects the preferential hydration of the protein and the nucleic acid versus their complex, i.e., it is a minimum number of water molecules involved in the reaction (*38*, *39*). Using this assumption, Figure 5b shows the dependence of the logarithm of the overall binding constant, K_{16}, of the PriA helicase−ssDNA 16-mer complex, upon the logarithm of the water concentration. The plot is linear and characterized by the slopes $\partial \log K_{16}/\partial \log[H_2O] = 1.7 \pm 0.3$. Thus, the value of the slope indicates that there is a minimum net uptake of ∼2 water molecules in the overall binding process.

The effect of glycerol on the kinetics of the PriA interactions with the ssDNA has been addressed in stopped-flow experiments, performed in the way analogous to the studies of the ssDNA length and salt effect described above. The obtained values of all kinetic and spectroscopic parameters are included in Table 3. The dependence of the logarithm of the overall partial equilibrium constant, K_I, characterizing the bimolecular step, upon the logarithm of $[H_2O]$ is included in Figure 5b. The plot is linear in the examined glycerol concentration range and the positive slope of the plot is $\partial \log K_I/\partial \log[H_2O] = 3.7 \pm 0.5$. This value is significantly larger than the one obtained for the overall binding process and indicates that the uptake of a minimum of ∼4 water molecules accompanies the initial association of the protein with the ssDNA. The log−log plots for the equilibrium constant, K_2, and the rate constants, k_2 and k_{-2}, are shown in Figure 5c. Contrary to K_I, the log−log plot for K_2 is characterized by the negative slope, $\partial \log K_2/\partial \log[H_2O] = -3 \pm 0.5$, indicating a net release of a minimum of ∼3 H_2O molecules in the formation of the $(P)_2$ intermediate. The slopes for the corresponding rate constants are $\partial \log k_2/\partial \log[H_2O] = -0.4 \pm 0.1$ and $\partial \log k_{-2}/\partial \log[H_2O] = 2.7 \pm 0.5$. Thus, although some water is released in the formation of the transition state, the majority of the H_2O molecules, released in the formation of the $(P)_2$ intermediate, seems to occur in the transformation from the transition state to the intermediate (see Discussion). The dependences of logarithms of K_3 and rate constants, k_3 and k_{-3}, characterizing the transition $(P)_2 \leftrightarrow (P)_3$ transition, upon the logarithm of $[H_2O]$ are shown in Figure 5d. The slopes of the log−log plots are $\partial \log K_3/\partial \log[H_2O] = -1.3 \pm 0.5$, $\partial \log k_3/\partial \log[H_2O] \approx 0$, and $\partial \log k_{-3}/\partial \log[H_2O] = 1.3 \pm 0.5$. Thus, the

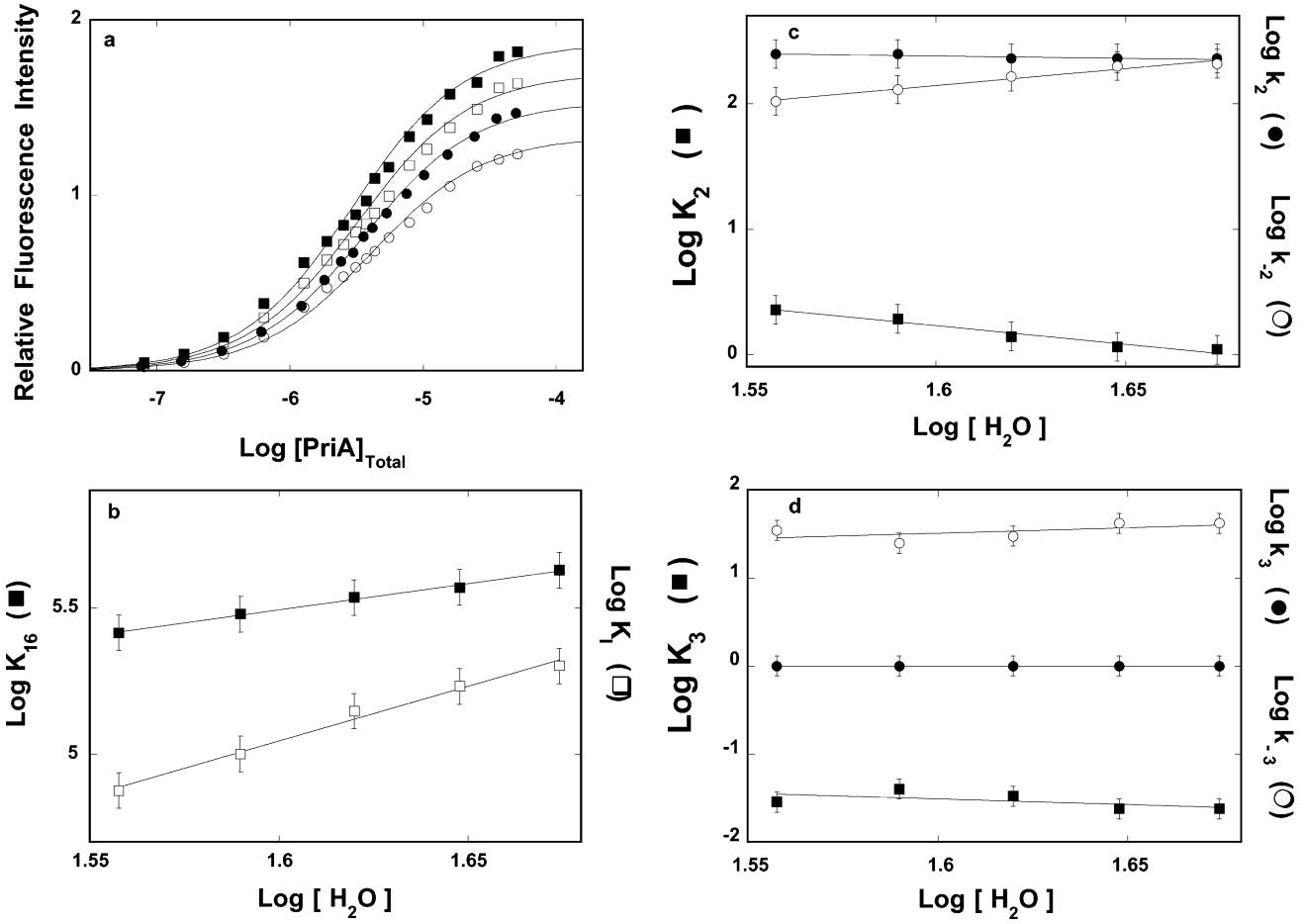

FIGURE 5: (a) Fluorescence titrations of the 16-mer, dϵA(pϵA)$_{15}$, with the PriA protein (λ_{ex} = 325 nm, λ_{em} = 410 nm) in buffer C (pH 7.0, 10 °C), containing 100 mM NaCl and different glycerol concentrations (%, w/v): (■) 20%, (□) 25%, (●) 30%, (○) 35%. The solid lines are computer fits of the titration curves, using a single-site binding isotherm (eq 7). The obtained binding parameters are included in Table 3. (b) The dependence of the logarithm of the overall equilibrium constant, K_{16} (■) and overall partial equilibrium constant, K_I (□), characterizing the bimolecular step for the PriA helicase binding to the ssDNA 16-mer, dϵA(pϵA)$_{15}$, (Scheme 1) upon the log[H_2O] (log−log plots). The plots are characterized by the slopes $\partial \log K_{16}/\partial \log[H_2O] = 1.7 \pm 0.3$, and $\partial \log K_I/\partial \log[H_2O] = 3.7 \pm 0.5$, respectively. (c) The dependence of the logarithm of the partial equilibrium constant, K_2 (■) and rate constants, k_2 (●) and k_{-2} (○), (Scheme 1) characterizing the first intramolecular step $(P)_1 \leftrightarrow (P)_2$, in the binding of the PriA helicase to the ssDNA 16-mer, dϵA(pϵA)$_{15}$, upon the log[NaCl]. The plots are characterized by the slopes $\partial \log K_2/\partial \log[H_2O] = -3 \pm 0.5$, $\partial \log k_2/\partial \log[H_2O] = -0.4 \pm 0.1$, $\partial \log k_{-2}/\partial \log[H_2O] = 2.7 \pm 0.5$. (d) The dependence of the logarithm of the partial equilibrium constant, K_3 (■) and rate constants, k_3 (●) and k_{-3} (○), (Scheme 1) characterizing the second intramolecular step $(P)_2 \leftrightarrow (P)_3$, in the binding of the PriA helicase to the ssDNA 16-mer, dϵA(pϵA)$_{15}$, upon the log[H_2O]. The plots are characterized by the slopes $\partial \log K_3/\partial \log[H_2O] = -1.3 \pm 0.5$, $\partial \log k_3/\partial \log[H_2O] = 0$, $\partial \log k_{-3}/\partial \log[NaCl] = 1.3 \pm 0.5$.

Table 3: Kinetic, Thermodynamic, and Spectroscopic Parameters Characterizing the Binding of the PriA Helicase to the ssDNA Oligomer, dϵA(pϵA)$_{15}$, in Buffer C (100 mM NaCl, 10 °C), Containing Different Concentrations of Glycerol

[glycerol] (%)	K_{eq}[a] (M^{-1})	ΔF_{max}[a]	K_1 (M^{-1})	k_2 (s^{-1})	k_{-2} (s^{-1})	k_3[b] (s^{-1})	k_{-3}[b] (s^{-1})	K_2	K_3	K_{16} (M^{-1})	F_2[c]	F_3[c]	F_4[c]
15			$(2.0 \pm 0.5) \times 10^5$	230 ± 40	210 ± 30	1	42 ± 8	1.1 ± 0.4	0.024 ± 0.01	$(4.24 \pm 1.3) \times 10^5$	1.02 ± 0.03	2.6 ± 0.1	6 ± 0.3
20	$(3.7 \pm 0.4) \times 10^5$	1.87 ± 0.11	$(1.7 \pm 0.5) \times 10^5$	230 ± 40	200 ± 30	1	42 ± 8	1.2 ± 0.4	0.024 ± 0.01	$(3.7 \pm 1.2) \times 10^5$	1.02 ± 0.03	2.5 ± 0.1	6.5 ± 0.3
25	$(3.3 \pm 0.4) \times 10^5$	1.7 ± 0.11	$(1.4 \pm 0.4) \times 10^5$	230 ± 40	165 ± 30	1	30 ± 7	1.4 ± 0.4	0.033 ± 0.011	$(3.42 \pm 1.1) \times 10^5$	1.02 ± 0.03	2.1 ± 0.1	4.3 ± 0.3
30	$(3.0 \pm 0.4) \times 10^5$	1.54 ± 0.11	$(1.0 \pm 0.3) \times 10^5$	250 ± 40	130 ± 25	1	25 ± 7	1.9 ± 0.7	0.040 ± 0.012	$(3.0 \pm 1.1) \times 10^5$	1.02 ± 0.03	1.8 ± 0.1	2.8 ± 0.2
35	$(2.61 \pm 0.3) \times 10^5$	1.34 ± 0.11	$(7.5 \pm 2.5) \times 10^5$	250 ± 40	105 ± 25	1	35 ± 8	2.3 ± 1	0.029 ± 0.012	$(2.6 \pm 0.9) \times 10^5$	1.02 ± 0.03	1.45 ± 0.08	2.6 ± 0.2

[a] Determined in independent fluorescence titrations. [b] Maximum estimated value. [c] Values relative to the fluorescence, $F_1 = 1$ of the free dϵA(pϵA)$_{15}$ (details in text).

formation of $(P)_3$ is accompanied by the net water molecule release occurring predominantly in the transformation from the transition state to the final $(P)_3$ intermediate. The effect of the increased glycerol concentration on the amplitudes of the observed intermediates parallels the effect observed for the salt (see above). However, the effect is much less pronounced. In the examined [glycerol], the fluorescence intensity of the $(P)_2$, F_3, is decreased from 2.6 ± 0.1 to 1.45

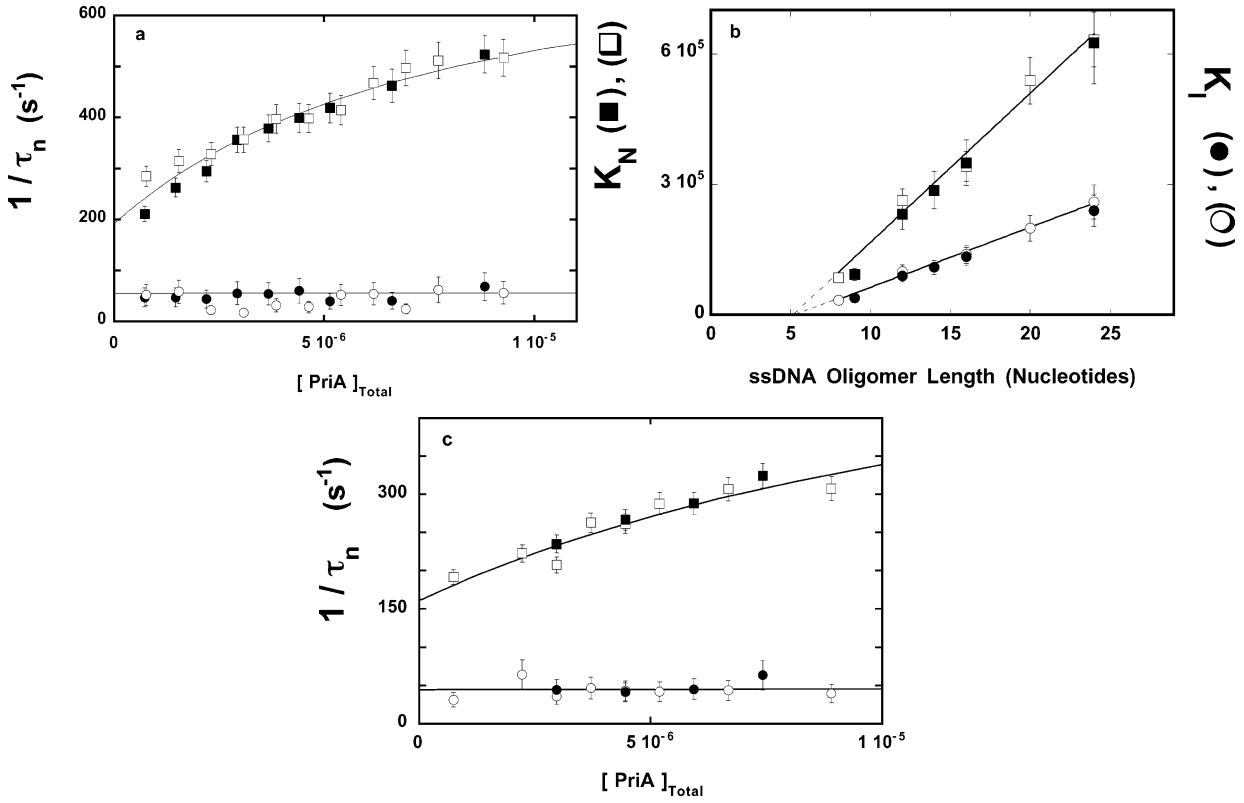

FIGURE 6: (a) The dependence of the reciprocal relaxation times, $1/\tau_1$ (■) and $1/\tau_2$ (●) for the binding of the PriA helicase to the ssDNA 16-mer, dϵA(pϵA)$_{15}$, in buffer C (pH 7.0, 10 °C), containing 100 mM NaCl and 2×10^{-4} M $MgCl_2$, upon the total concentration of the enzyme. The analogous plot for the relaxation time, τ_1, obtained in the presence of 1×10^{-4} M EDTA and in the absence of $MgCl_2$, is also included ($1/\tau_1$ (□), $1/\tau_2$ (○)). The solid line is the nonlinear least-squares fit according to the three-step sequential mechanism, defined by Scheme 1, for the data obtained in the absence of magnesium, with the overall partial equilibrium constant $K_I = 1.4 \times 10^5$ M^{-1} and the rate constants: $k_2 = 230$ s^{-1}, $k_{-2} = 165$ s^{-1}, $k_3 = 1$ s^{-1}, and $k_{-3} = 30$ s^{-1} (Table 1). (b) The dependence of the overall equilibrium constant K_N, (■) and overall partial equilibrium constant K_I, (●) characterizing the bimolecular step (Scheme 1), for PriA binding to ssDNA oligomers with different number of nucleotide residues, in buffer C (pH 7.0, 10 °C), containing 100 mM NaCl and 2×10^{-4} M $MgCl_2$, upon the length of the ssDNA oligomer (Nucleotides), superimposed on the analogous plot (K_N, (□), K_I, (○)) obtained in the absence of magnesium (Figure 3b). (c) The dependence of the reciprocal relaxation times, $1/\tau_1$ (■) and $1/\tau_2$ (●) for the binding of the PriA helicase to the ssDNA 16-mer, dϵA(pϵA)$_{15}$, in buffer C (pH 7.0, 10 °C), containing 100 mM NaCl, 5 mM $MgCl_2$, and 1 mM AMP−PNP, upon the total concentration of the enzyme. Analogous plots for the reciprocal relaxation time, $1/\tau_1$ (□) and $1/\tau_2$ (○), obtained in the absence of AMP−PNP, are also included. The solid line is the nonlinear least-squares fit according to the three-step sequential mechanism, defined by Scheme 1, with the overall partial equilibrium constant $K_I = 6.5 \times 10^5$ M^{-1} and the rate constants: $k_2 = 230$ s^{-1}, $k_{-2} = 160$ s^{-1}, $k_3 = 1$ s^{-1}, and $k_{-3} = 45$ s^{-1}.

± 0.08 while the fluorescence intensity of the $(P)_3$ intermediate, F_4, decreases from 6 ± 0.3 to 2.6 ± 0.2 (Table 3) (see Discussion).

Mechanism of PriA Binding to the ssDNA in the Presence of Mg^{2+} Cations and AMP−PNP. The effect of the magnesium cations on the kinetic mechanism of the PriA helicase binding to the ssDNA has been examined using the ssDNA 16-mer, dϵA(pϵA)$_{15}$, in analogous way as described above, however, in buffer C (pH 7.0, 10 °C), containing 100 mM NaCl, 2×10^{-4} M $MgCl_2$, and no EDTA. The concentration of $MgCl_2$ was selected to saturate the cation-binding site on the protein, without affecting the ionic strength of the solution (*29*). The two-exponential fit provides an excellent representation of the observed kinetic traces, indicating that the overall relaxation process is described by the kinetic mechanism defined by Scheme 1 (data not shown). The dependence of the reciprocal relaxation times, $1/\tau_1$ and $1/\tau_2$ upon the total concentration of PriA, is shown in Figure 6a. For comparison, the dependence of the same relaxation times, obtained in the presence of EDTA (Figure 3a), upon the total [PriA] is also included in Figure 6a. Within experimental accuracy, both relaxation times have the same values and functional dependence upon the protein concentration as observed in the presence of EDTA and in the absence of magnesium cations. In other words, the presence of Mg^{2+} does not affect the mechanism and values of the rate constants characterizing the particular steps of the reaction.

To address the problem of whether the magnesium affects the site-size of the ssDNA-binding site of the PriA helicase, we performed stopped-flow experiments with a series of the ssDNA oligomers, dϵA(pϵA)$_8$, dϵA(pϵA)$_{11}$, dϵA(pϵA)$_{13}$, dϵA(pϵA)$_{15}$, and dϵA(pϵA)$_{23}$, in the same way as described above for experiments performed in the absence of Mg^{2+} (Figure 3a,b). Figure 6b shows the overall equilibrium constant, K_N, and the overall partial equilibrium constant, K_I, for PriA binding to ssDNA oligomers, 9-, 12-, 14-, 16-, and 24-mer, as functions of the ssDNA oligomer length, obtained in buffer C (pH 7.0, 10 °C), containing 100 mM NaCl, 2×10^{-4} M $MgCl_2$, and no EDTA. For comparison, the same binding parameters, determined in the absence of magnesium, are included (Figure 3b). Similar to the behavior of the rate parameters (Figure 6a), both K_N and K_I show, within experimental accuracy, the same dependence upon the length of the ssDNA oligomer as observed in the absence of Mg^{2+}.

Thermodynamic studies indicated that the presence of ATP nonhydrolyzable analogue, AMP−PNP, has little effect on

the PriA binding to the ssDNA (*29*). In the final set of experiments, we examined the kinetics of the PriA binding to the ssDNA 16-mer, dϵA(pϵA)$_{15}$, in the absence and presence of AMP−PNP. The stopped-flow studies were performed in buffer C (pH 7.0, 10 °C), containing 100 mM NaCl and 5 mM $MgCl_2$. As in all examined conditions, the observed kinetic traces were adequately represented by two-exponential function, indicating that the overall relaxation process is described by the kinetic mechanism defined by Scheme 1 (data not shown). The dependence of the reciprocal relaxation times, $1/\tau_1$ and $1/\tau_2$, upon the total concentration of PriA, in the absence and presence of AMP−PNP is shown in Figure 6c. Both plots are superimposable and provide very similar values of rate constants and spectroscopic parameters characterizing intermediates. These data clearly show that the nucleotide cofactor does not affect the mechanism of the PriA binding and the internal dynamics of the helicase−ssDNA complex.

DISCUSSION

Multiple-Step Kinetic Mechanism of PriA Helicase Binding to the ssDNA. The results obtained in this work indicate that the mechanism of the PriA binding to the ssDNA is a minimum three-step, sequential process described by Scheme 1. The resolved relaxation times have a dependence upon the enzyme concentration typical for intramolecular transitions (*34*, *35*). Thus, the enzyme−ssDNA complex undergoes at least two conformational transitions following the initial bimolecular step. The bimolecular step is too fast to be resolved in stopped-flow measurements, independently of the length of the ssDNA oligomer. This behavior indicates that the fast initial binding of the PriA helicase is an intrinsic property of the PriA−ssDNA system. The amplitude analyses show that there is very little, if any, change of the nucleic acid fluorescence accompanying the formation of the $(P)_1$ intermediate (Scheme 1).

Interpretation of the fluorescence changes of etheno-ssDNA oligomers is facilitated by the fact that dramatic quenching of the nucleic acid fluorescence is well understood in terms of intramolecular collisions due to the motion of ϵA separated by a close distance in the DNA (*23*, *40*). Thus, the extent of the fluorescence increase in the protein−nucleic acid complexes reflects the conformational changes of the nucleic acid (immobilization and separation of bases) that limits these quenching processes (*23*, *40*). The lack of detectable fluorescence change in $(P)_1$ indicates that the ssDNA conformation is very similar to the conformation of the free DNA, i.e., unaffected by the protein binding. This is an expected behavior for a collision complex (*41*, *42*). However, very fast protein/nucleic acid conformational change, occurring in the formation of $(P)_1$, cannot be completely excluded on the basis of stopped-flow measurements alone.

The step following the bimolecular association (Scheme 1) is also fast and characterized by the forward rate constant, $k_2 \sim 250\ s^{-1}$ at 100 mM NaCl (Table 1). The backward rate constant, k_{-2}, is $\sim 150\ s^{-1}$; thus, the step provides very modest additional stabilization of the protein−ssDNA complex. Nevertheless, the values of k_2 and k_{-2} indicate that the lifetime of the $(P)_2$ intermediate is in the range of several milliseconds. Moreover, amplitude analyses show that, contrary to the $(P)_1$ intermediate, the formation of $(P)_2$ is accompanied by a strong nucleic acid fluorescence increase, indicating large changes in the DNA structure in the complex. These data indicate that in the second step, the adjustment of the ssDNA conformation to the structure of the binding site occurs, i.e., it is the recognition step in the binding process (see above). Although the subsequent transition to the $(P)_3$ intermediate is also accompanied by a strong conformational change of the nucleic acid, it is energetically very unfavorable and, as a result, contributes very little to the total population of the helicase−DNA complexes (Table 1). Kinetics of the nucleotide hydrolysis or the dsDNA unwinding by the PriA helicase are unknown. However, the favorable free energy change of the $(P)_1 \leftrightarrow (P)_2$ transition, adjustment of the DNA structure to the structure of the DNA-binding site, and the lifetime of the complex in the range of milliseconds suggest that the $(P)_2$ and not the $(P)_3$ intermediate may play an important role in the catalysis.

Dependence of the Dynamics of the PriA−ssDNA Complex Formation Upon the Length of the ssDNA Indicates That the Strong DNA-Binding Site of the Enzyme, Encompassing ~6 Nucleotide Residues, Is Exclusively Involved in Interactions with the Nucleic Acid. As mentioned above, thermodynamic studies showed that the total site-size of the PriA−ssDNA complex is 20 ± 3 nucleotide residues (*19*, *20*). However, the DNA-binding site, located in the central part of the helicase molecule, occludes only 8 ± 1 residues (*19*, *20*). In other words, the protein matrix extends over ~6 residues on both sides of the binding site, without engaging in interactions with the DNA. Therefore, if the protein matrix outside the strong binding site does not engage in interactions with the DNA, for any ssDNA oligomer longer than ~8 nucleotide residues, the overall binding constant K_N and the overall partial equilibrium constant, K_I, characterizing the bimolecular step, must contain a factor $N - n + 1$ resulting from the existence of $N - n + 1$ potential binding sites (eqs 4a, 4b, and 4c) (*43*, *44*). On the other hand, the partial equilibrium constants K_2 and K_3 should be independent of the length of the ssDNA oligomers. Both thermodynamic and kinetic analyses clearly show that the dependence of K_N and K_I upon the length of ssDNA oligomers strictly follows the predicted linear dependence upon N (Figures 3b and 6b), while partial equilibrium constants characterizing intramolecular steps are, within experimental accuracy, independent of N (Table 1). Such behavior could only be observed if the strong DNA-binding site of the PriA helicase is exclusively involved in interactions with the ssDNA.

The plot of K_N and K_I intercept the oligomer length axis at $n = 6.3 \pm 1$ indicating that the ssDNA-binding site of the helicase encompasses ~2 nucleotide residues less than determined in thermodynamic analyses (*19*, *20*). This difference should not be surprising. The shortest length of the ssDNA oligomer that can be accessed in direct thermodynamic studies corresponds to the shortest oligomer whose binding can still be detected, i.e., eight nucleotide residues. Combined application of the thermodynamic and kinetic studies provides a much more accurate estimate of the size of the strong ssDNA binding site. The linear dependence of only K_N upon N, does not establish the existence of a purely statistical effect in the observed increase of the overall binding constant. On the other hand, the linear dependence of both K_N and K_I and the common interception point on

the ssDNA oligomer length axis (Figure 3b) constitute a very strong evidence that the observed increase of both equilibrium binding constants with the length of the ssDNA oligomer results from the statistical effect of the potential binding sites. It also indicates that a ssDNA patch of ~6 nucleotide residues in length is absolutely necessary for the enzyme to form a stable complex with the ssDNA and confirms the lack of any "end effect" in the PriA binding to the ssDNA, previously determined in thermodynamic studies (*19*, *20*).

In this context, it is not surprising that dynamics of the enzyme binding to various ssDNA oligomers in subsequent steps, $(P)_1 \leftrightarrow (P)_2$ and $(P)_2 \leftrightarrow (P)_3$, are independent of the length of the oligomers. It simply means that, as long as the stretch of ~6 nucleotide residues of the ssDNA is available, and a stable $(P)_1$ intermediate is formed, it undergoes similar transitions, little dependent on the surrounding nucleic acid. This is because the protein matrix, outside the ssDNA-binding site, does not engage in interactions with the ssDNA. However, amplitude analyses indicate that molecular fluorescence intensities characterizing intermediates, $(P)_2$ and $(P)_3$, are different among different ssDNA oligomers (Table 2). Recall that the molecular fluorescence intensities characterize the relative fluorescence change of the entire ssDNA oligomer with respect to the same free DNA (see above). Because the enzyme associates with the ssDNA using only its ssDNA-binding site, these data indicate that the conformational transitions of the nucleic acid, generated at the ssDNA-binding site−ssDNA interface, extend to the rest of the bound nucleic acid molecule, although part of the ssDNA is not involved in direct interactions with the helicase (*19*, *20*).

Salt and Glycerol Effects on the PriA−ssDNA Kinetics Indicate that Ion Binding Stabilize the Helicase−ssDNA Complex in $(P)_2$ and $(P)_3$ Intermediates. Clear indication of the very different nature of the formed intermediates comes from the examination of the salt and glycerol effects on the kinetics of PriA−ssDNA interactions. The bimolecular step is accompanied by a net release of $\partial \log K_1/\partial \log[\mathrm{NaCl}] = -4.2 \pm 0.3$ ions, significantly larger than the net ion release, $m = \partial \log K_{16}/\partial \log[\mathrm{NaCl}] = -2.8 \pm 0.3$, observed in the overall binding process. Recall that thermodynamic studies showed that the overall net ion release accompanying PriA−ssDNA interactions is not dependent upon the type of anion in solution, indicating that only cations participate in the ion exchange process (*36*, *37*). Moreover, the bimolecular step is close to a collision process, and there is very little nucleic acid conformational change accompanying the formation of the $(P)_1$ intermediate (see above). These data would suggest that ions released in the formation of the first intermediate between the helicase and the ssDNA are territorially bound cations, exclusively released from the nucleic acid (*36*, *37*). However, the effect of glycerol on the bimolecular step of the PriA−ssDNA complex formation strongly suggests an uptake of ~4 water molecules in the process (Figure 5). The uptake of water in the bimolecular step is surprising. Rather, the release of water would be expected to be a part of the entropic contribution to the free energy of association (*45*, *46*). The simplest explanation of the observed water uptake is that some of the released cations are partially dehydrated in the bound state, i.e., they originated from the protein, and rebuild their hydration layers after the release from the protein.

Contrary to the bimolecular step, the $(P)_1 \leftrightarrow (P)_2$ and $(P)_2 \leftrightarrow (P)_3$ transitions are accompanied by a net uptake of ~2 and ~1 ion, respectively (Figure 4). In the case of the $(P)_1 \leftrightarrow (P)_2$ step, ion binding affects the formation of the activated complex and its transition to the $(P)_2$ intermediate, indicating that the ion-binding sites of a different nature are involved (see below). In both $(P)_1 \leftrightarrow (P)_2$ and $(P)_2 \leftrightarrow (P)_3$ steps, the protein−ssDNA complex undergoes significant conformational changes as reflected in large fluorescence changes of the nucleic acid (Table 2). The observed uptake of ions provides an additional stabilization of both intermediates, most probably, to stabilize interactions with the induced nucleic acid conformation. Notice that the intramolecular steps are accompanied by water release characterized by the slopes, $\partial \log K_2/\partial \log[H_2O] = -3 \pm 0.5$ and $\partial \log K_3/\partial \log[H_2O] = -1.3 \pm 0.5$, respectively (Figure 5). Thus, this behavior is exactly opposite to the ion effect on both intramolecular steps. Moreover, the water release occurs in the same transitions where the ion binding occurs, however, predominantly, in the transitions from the activated complex to the following intermediates (Figures 4 and 5). Such behavior suggests that, at least partially, the released water molecules originate from the dehydration of the bound ions in the transition from the activated complex to the following intermediate. This result provides additional support for the conclusion that the observed ion binding involves ion binding sites on the helicase. In this context, it should be noticed that the salt concentration has a strong effect on the molar fluorescence properties of the intramolecular intermediates, $(P)_2$ and $(P)_3$, but not on the bimolecular complex (Tables 3 and 3). Both F_3 and F_4 strongly decrease, particularly, at elevated [NaCl]. These data indicate that the transmission of structural changes, induced by the enzyme at the ssDNA-binding site, to the rest of the bound DNA molecule, not engaged in direct interactions with the helicase, is hindered by the ion binding. The effect is not linear and saturates at a [NaCl] ≈ 100 mM (Table 2), indicating that an ion binding process, characterized by the binding constant > 50 M^{-1}, is observed.

Sequential Mechanism Indicates that the PriA Helicase Does Not Exist in a Preequilibrium Conformational Transition prior to the ssDNA Binding. Kinetic analyses of the ligand binding are a very sensitive method to detect any preequilibrium conformational transitions of the macromolecule (*34*, *35*). In the case of PriA−ssDNA interactions, both relaxation times and amplitudes show behavior typical for a sequential mechanism of binding, i.e., without any preequilibrium conformational transition. Moreover, the number of relaxation times is independent of whether the experiments are performed in pseudo-first-order conditions with respect to the protein or DNA concentration (*30*, *31*). Therefore, the sequential mechanism of the PriA binding to the ssDNA provides a very strong indication that the enzyme does not exist in a preequilibrium conformational transition prior to the DNA binding. In other words, conformational changes of the PriA helicase in the complex with the ssDNA are induced by interactions with the nucleic acid.

ATP Analogue, AMP−PNP, Does Not Affect the Thermodynamics or Dynamics of the PriA Helicase Interactions with the ssDNA. A puzzling aspect of the PriA helicase

FIGURE 7: Schematic model of the PriA helicase − ssDNA complex. The proper DNA-binding site of the enzyme engages in interactions only $n = 6 \pm 1$ nucleotide residues. The site is located on a separated structural domain of the enzyme, most probably the helicase domain, which protrudes from the remaining protein matrix. Only the DNA-binding site engages in strong interactions the nucleic acid. The domain containing the DNA-binding site is placed in the central part of the helicase molecule. The protein matrix protrudes symmetrically on both sides of the strong ssDNA-binding site without engaging in interactions with the nucleic acid. As a result, the total site-size of the PriA helicase−ssDNA complex occludes is $n_t = 20 \pm 3$ nucleotide residues (*19*, *20*).

interactions with the ssDNA is the lack of any effect of nucleotide cofactors on the enzyme binding to the ssDNA (*20*). Experiments described in this work indicate that the ATP analogue, AMP−PNP, does not affect to any detectable extent either the dynamics of the interactions or the distribution of the formed intermediates. This behavior is very different from other well-studied helicases in which ATP is indispensable for the enzyme to bind to the ssDNA (*51*). The ATP binding/hydrolysis processes, allosterically controlling the enzyme affinity for the ssDNA, are thought to play a decisive role in the enzyme functioning. In this aspect, the PriA helicase seems to be very different from the, so far accepted, canonical model. However, it is possible that while interactions with the ssDNA are not affected, the nucleotide cofactors may play a role in the PriA binding to more complex DNA structures formed at the restarting replication fork (*17*, *18*).

Functional Implications. The Active, ssDNA-Searching Site of a Helicase. It is remarkable that, although the DNA binding site encompasses only 6.3 ± 1 nucleotide residues within ~20 nucleotide residues of the total site-size of the PriA−ssDNA complex, the surrounding protein matrix does not enter in thermodynamically and kinetically detectable interactions with the ssDNA in the examined nucleic acid and protein concentration ranges (*19*, *20*). The length dependence of the dynamics of the PriA binding to the ssDNA indicates that, even in the first intermediate $(P)_1$ between the protein and the DNA, only the DNA-binding site, but not the surrounding protein matrix, makes the first and only contact with the nucleic acid (Figure 3b). Moreover, the lack of any length effect on following intermediates $(P)_2$ and $(P)_3$ clearly indicates that the subsequent conformational transitions of the helicase−DNA complex do not engage the protein matrix, outside the DNA-binding site. This behavior can be understood in the context of the structural model of the PriA helicase, as schematically depicted in Figure 7. To achieve the experimentally observed independence from the rest of the enzyme molecule, the DNA-binding site must protrude from the remaining protein matrix. Although the three-dimensional structure of the PriA helicase is still unknown, the obtained data strongly suggest that the ssDNA-binding site is placed on a well-defined structural domain of the protein, most probably the helicase domain, located in the central part of the enzyme molecule.

In chromosomal DNA replication, the role of the PriA helicase seems to be predominantly related to the initiation of the restarting of DNA replication after the replication fork stalls, at the damaged DNA sites (*17*, *18*). The helicase activity of the protein would allow the unwinding of the duplex conformation of the lagging strand of the fork, preparing it for the binding of the DnaB helicase and assembling the preprimosome complex. Recent analyses of the enzyme activity on different synthetic DNA substrates strongly suggest that the enzyme requires short ssDNA gaps to initiate its helicase activity (*18*). In other words, the PriA helicase is able to efficiently search and recognize very short ssDNA gaps in the presence of an overwhelmingly large excess of the dsDNA conformation. In fact, the optimal length of the recognized ssDNA gap is ~5 nucleotide residues (*18*). It is clear that the data obtained in this work, indicating that the ssDNA-binding site occludes ~6 nucleotide residues, corroborate very well with these findings. Thus, the helicase active site is built to efficiently search small ssDNA patches, i.e., it protrudes from the rest of the protein molecule. Such structure of the active site would be an evolutionary adaptation of the PriA helicase to perform specific, ssDNA gap searching and recognition. Nevertheless, although the DNA-binding capability of the protein matrix, that occludes the remaining nucleotide residues of the total site-size, is not detectable, it may play an important role in orienting the enzyme within the specific DNA substrate structures, e.g., arrested replication fork structures. In such situations, when the local concentration of the DNA becomes very high, even low affinity binding sites may begin to play a role in the binding. As we noted above, these inherently weak interactions with more complex DNA structures may be under ATP/ADP binding/hydrolysis control. Our laboratory is currently examining these possibilities.

The very fast bimolecular step and the fast following recognition step make PriA binding to the ssDNA similar to other well-known, fast protein−nucleic acid recognition reactions, including aminoacyl-tRNA synthetases, ribosomal proteins, and mammalian DNA repair polymerase β (*32*, *33*, *47*−*49*). A common feature of these systems is that the enzyme/protein recognizes a specific nucleic acid substrate (sequence, specific nucleic acid structure, or both) among many substrates or within the context of several nonfunctional binding sites. Fast association and dissociation reaction in the first binding step and fast recognition step provide the protein with a means to quickly examine the structure of the encountered nucleic acid. As mentioned above, the PriA helicase is involved in restarting the DNA replication when the replication fork encounters the damaged DNA (*17*, *18*). Thus, very fast binding and recognition steps would allow the enzyme to efficiently recognize the specific ssDNA gap on the lagging strand and initiate the assembling of the preprimosome complex.

ACKNOWLEDGMENT

We wish to thank Betty Sordahl for reading the manuscript and Dr. Aaron Lucius for reading and commenting on the manuscript.

REFERENCES

1. Marians, K. J. (1992) Prokaryotic DNA replication, *Annu. Rev. Biochem. 61*, 673−719.

2. Marians, K. J. (1999) PriA: at the crossroads of DNA replication and recombination, *Prog. Nucleic Acid Res. Mol. Biol. 63*, 39−67.
3. Kornberg, A., and Baker, T. A. (1992) *DNA Replication*, pp 275−293, Freeman, San Francisco.
4. Wickner, S., and Hurwitz, J. (1974) Conversion of ϕiX174 viral DNA to double-stranded form by purified *Escherichia coli* proteins, *Proc. Natl. Acad. Sci. U.S.A. 71*, 4120−4124.
5. McMacken, R., Ueda, K., and Kornberg, A. (1977) Migration of *Escherichia coli* dnaB protein on the template DNA strand as a mechanism in initiating DNA replication, *Proc. Natl. Acad. Sci. U.S.A. 74*, 4190−4194.
6. Wickner, S., and Hurwitz, J. (1975) Association of phiX174 DNA-dependent ATPase activity with an *Escherichia coli* protein, replication factor Y, required for in vitro synthesis of phiX174 DNA, *Proc. Natl. Acad. Sci. U.S.A. 72*, 3342−3346.
7. Shlomai, J., and Kornberg, A. (1980) A prepriming DNA replication enzyme of *Escherichia coli*. I. Purification of protein n′: a sequence-specific, DNA-dependent ATPase, *J. Biol. Chem. 255*, 6789−6793.
8. Zipursky, S. L., and Marians, K. J. (1980) Identification of two *Escherichia coli* factor Y effector sites near the origins of replication of the plasmids ColE1 and pBR322, *Proc. Natl. Acad. Sci. U.S.A. 77*, 6521−6525.
9. Shlomai, J., and Kornberg, A. (1980) A prepriming DNA replication enzyme of *Escherichia coli*. II. Actions of protein n′: a sequence-specific, DNA-dependent ATPase, *J. Biol. Chem. 255*, 6794−6798.
10. Marians, K. J., Soeller, W., and Zipursky, S. L. (1982) Maximal limits of the *Escherichia coli* replication factor Y effector site sequences in pBR322 DNA, *J. Biol. Chem. 257*, 5656−5662.
11. Lee, M. S., and Marians, K. J. (1987) *Escherichia coli* replication factor Y, a component of the primosome, can act as a DNA helicase, *Proc. Natl. Acad. Sci. U.S.A. 84*, 8345−8349.
12. Lasken, R. S., and Kornberg, A. (1988) The primosomal protein n′ of *Escherichia coli* is a DNA helicase, *J. Biol. Chem. 263*, 5512−5518.
13. Nurse, P., DiGate, R. J., Zavitz, K. H., and Marians, K. J. (1990) Molecular cloning and DNA sequence analysis of *Escherichia coli* priA, the gene encoding the primosomal protein replication factor Y, *Proc. Natl. Acad. Sci. U.S.A. 87*, 4615−4619.
14. Lee, E. H., Masai, H., Allen, G. C., Jr., and Kornberg, A. (1990) The priA gene encoding the primosomal replicative n′ protein of *Escherichia coli*, *Proc. Natl. Acad. Sci. U.S.A. 87*, 4620−4624.
15. McGlynn, P., Al-Deib, A. A., Liu, J., Marians, K. J., and Lloyd, R. G. (1997) The DNA replication protein PriA and the recombination protein RecG bind D-loops, *J. Mol. Biol. 270*, 212−221.
16. Nurse, P., Liu, J., and Marians, K. J. (1999) Two modes of PriA binding to DNA, *J. Biol. Chem. 274*, 25026−25032.
17. Jones, J. M., and Nakai, H. (1999) Duplex opening by primosome protein PriA for replisome assembly on a recombination intermediate, *J. Mol. Biol. 289*, 503−516.
18. Jones, J. M., and Nakai, H. (2001) *Escherichia coli* PriA helicase: fork binding orients the helicase to unwind the lagging strand side of arrested replication forks, *J. Mol. Biol. 312*, 935−947.
19. Jezewska, M. J., Rajendran, S., and Bujalowski, W. (2000) *Escherichia coli* replicative helicase PriA protein-single-stranded DNA complex. Stoichiometries, free energy of binding, and cooperativities, *J. Biol. Chem. 275*, 27865−27873.
20. Jezewska, M. J., and Bujalowski, W. (2000) Interactions of *Escherichia coli* replicative helicase PriA protein with single-stranded DNA, *Biochemistry 39*, 10454−10467.
21. Secrist, J. A., 3rd, Barrio, J. R., Leonard, N. J., and Weber, G. (1972) Fluorescent modification of adenosine-containing coenzymes. Biological activities and spectroscopic properties, *Biochemistry 11*, 3499−3506.
22. Ledneva, R. K., Razjivin, A. P., Kost, A. A., and Bogdanov, A. A. (1978) Interaction of tobacco mosaic virus protein with synthetic polynucleotides containing a fluorescent label: optical properties of poly(ϵA) and poly(ϵC) copolymers and energy migration from the tryptophan to 1,N^6-ethenoadenine or 3,N^4-ethenocytosine residues in RNP, *Nucleic Acids Res. 5*, 4225−4243.
23. Tolman, G. L., Barrio, J. R., and Leonard, N. J. (1974) Chloroacetaldehyde-modified dinucleoside phosphates. Dynamic fluorescence quenching and quenching due to intramolecular complexation, *Biochemistry 13*, 4869−4878.
24. Bujalowski, W., and Klonowska, M. M. (1994) Structural characteristics of the nucleotide-binding site of *Escherichia coli* primary replicative helicase DnaB protein. Studies with ribose and base-modified fluorescent nucleotide analogs, *Biochemistry 33*, 4682−4694.
25. Bujalowski, W., and Jezewska, M. J. (1995) Interactions of *Escherichia coli* primary replicative helicase DnaB protein with single-stranded DNA. The nucleic acid does not wrap around the protein hexamer, *Biochemistry 34*, 8513−8519.
26. Edeldoch, H. (1967) Spectroscopic Determination of Tryptophan and Tyrosine in Proteins, *Biochemistry 6*, 1948−1954.
27. Gill, S. C., and von Hippel, P. H. (1989) Calculation of protein extinction coefficients from amino acid sequence data, *Anal. Biochem. 182*, 319−326.
28. Bujalowski, W., and Jezewska, M. J. (2000) Kinetic mechanism of the single-stranded DNA recognition by *Escherichia coli* replicative helicase DnaB protein. Application of the matrix projection operator technique to analyze stopped-flow kinetics, *J. Mol. Biol. 295*, 831−852.
29. Bujalowski, W., and Jezewska, M. J. (2000) Kinetic mechanism of nucleotide cofactor binding to *Escherichia coli* replicative helicase DnaB protein. stopped-flow kinetic studies using fluorescent, ribose-, and base-modified nucleotide analogues, *Biochemistry 39*, 2106−2122.
30. Galletto, R., and Bujalowski, W. (2002) The *Escherichia coli* replication factor DnaC protein exists in two conformations with different nucleotide binding capabilities. I. Determination of the binding mechanism using ATP and ADP fluorescent analogues, *Biochemistry 41*, 8907−8920.
31. Galletto, R., and Bujalowski, W. (2002) Kinetics of the *Escherichia coli* replication factor DnaC protein-nucleotide interactions. II. Fluorescence anisotropy and transient, dynamic quenching stopped-flow studies of the reaction intermediates, *Biochemistry 41*, 8921−8934.
32. Rajendran, S., Jezewska, M. J., and Bujalowski, W. (2001) Multiple-step kinetic mechanisms of the ssDNA recognition process by human polymerase β in its different ssDNA binding modes, *Biochemistry 40*, 11794−11810.
33. Jezewska, M. J., Galletto, R., and Bujalowski, W. (2002) Dynamics of gapped DNA recognition by human polymerase β, *J. Biol. Chem. 277*, 20316−20327.
34. Bernasconi, C. J. (1976) *Relaxation Kinetics*, pp 20−39, Academic Press, NY.
35. Hammes, G. G., and Schimmel, P. R. (1970) *The Enzymes. Kinetics and Mechanism*, Vol. II, pp 67−114, Academic Press, New York.
36. Record, M. T., Jr., Anderson, C. F., and Lohman, T. M. (1978) Thermodynamic analysis of ion effects on the binding and conformational equilibria of proteins and nucleic acids: the roles of ion association or release, screening, and ion effects on water activity, *Q. Rev. Biophys. 11*, 103−178.
37. Record, M. T., Lohman, T. M., and deHaseth, P. L. (1976) Ion effects on ligand−nucleic acid interactions, *J. Mol. Biol. 107*, 145−158.
38. Timasheff, S. N. (1998) In disperse solution, "osmotic stress" is a restricted case of preferential interactions, *Proc. Natl. Acad. Sci. U.S.A. 95*, 7363−7367.
39. Timasheff, S. N. (1995) *Protein−Solvent Interactions*, pp 445−482, Gregory, R. B., Ed.; M. Dekker, New York.
40. Baker, B. M., Vanderkooi, J., and Kallenbach, N. R. (1978) Base stacking in a fluorescent dinucleotiside monophosphate: ϵApϵA, *Biopolymers 17*, 1361−1372.
41. Connors, K. W. (1990) *Chemical Kinetics. The Study of Reaction Rates in Solution*, pp 133−186, VCH, New York.
42. Berry, R. S., Rice, S. A., and Ross, J. (1980) *Physical Chemistry*, pp 1117−1204, J. Wiley & Sons, N. Y.
43. McGhee, J. D., and von Hippel, P. H. (1974) Theoretical aspects of DNA-protein interactions: cooperative and noncooperative binding of large ligands to a one-dimensional homogeneous lattice, *J. Mol. Biol. 86*, 469−489.
44. Epstein, I. R. (1978) Cooperative and noncooperative binding of large ligands to a finite one-dimensional lattice. A model for ligand-oligonucleotide interactions, *Biophys. Chem. 8*, 327−239.
45. Tanford, C. (1969) Extension of the theory of linked functions to incorporate the effects of protein hydration, *J. Mol. Biol. 39*, 539−544.
46. Spolar, R. S., and Record, M. T., Jr. (1994) Coupling of local folding to site-specific binding of proteins to DNA, *Science 263*, 777−784.

47. Mulsch, A., Colpan, M., Wollny, E., Gassen, H. G., and Riesner, D. (1981) Mechanism of the interaction between ribosomal protein S1 and oligonucleotides, *Nucleic Acids Res. 9*, 2367−2385.
48. Riesner, D., Pingoud, A., Boehme, D., Peters, F., and Maass, G. (1976) Distinct steps in the specific binding of tRNA to aminoacyl-tRNA synthetase. Temperature-jump studies on the serine-specific system from yeast and the tyrosine-specific system from *Escherichia coli*, *Eur. J. Biochem. 68*, 71−80.
49. Jezewska, M. J., Galletto, R., and Bujalowski, W. (2003) Rat polymerase β gapped DNA interactions: antagonistic effects of the 5′ terminal PO^{4-} group and magnesium on the enzyme binding to the gapped DNAs with different ssDNA gaps, *Cell Biochem. Biophys. 38*, 125−160.
50. Lohman, T. M., and Bjornson, K. P. (1996) Mechanisms of helicase-catalyzed DNA unwinding, *Annu. Rev. Biochem. 65*, 169−214.
51. Patel, S. S., and Picha, K. M. (2000) Structure and function of hexameric helicases, *Annu. Rev. Biochem. 69*, 651−697.

BI049378Q